Human Primary Liver Cancer -derived Organoid Cultures for disease modelling and drug screening

Laura Broutier[1], Gianmarco Mastrogiovanni#[1,3], Monique M.A. Verstegen#[2], Hayley E. Francies#[4], Lena Morrill Gavarró[3], Charles R Bradshaw[1], George E Allen[1], Robert Arnes-Benito[1], Olga Sidorova[1], Marcia P. Gaspersz[2], Nikitas Georgakopoulos[5], Bon-Kyoung Koo[3], Sabine Dietmann[3], Susan E. Davies[6], Raaj K. Praseedom[7], Ruby Lieshout[2], Jan N. M. IJzermans[2], Stephen J Wigmore[8], Kourosh Saeb-Parsy[5], Mathew J. Garnett[4], Luc J.W. van der Laan[2], Meritxell Huch[1,3,9*]

(1) The Wellcome Trust/CRUK Gurdon Institute, University of Cambridge, UK.
(2) Department of Surgery, Erasmus MC-University Medical Center, Rotterdam, Netherlands.
(3) Wellcome Trust - Medical Research Council Stem Cell Institute, University of Cambridge, UK.
(4) Wellcome Trust Sanger Institute, Wellcome Trust Genome Campus, Hinxton, UK.
(5) Department of Surgery, University of Cambridge and NIHR Cambridge Biomedical Research Centre, Cambridge, UK.
(6) Department of Histopathology, Cambridge University Hospitals NHS Foundation Trust, Cambridge, UK.
(7) Department of Hepato Pancreato Biliary Surgery, Cambridge University Hospitals NHS Foundation Trust, Cambridge, UK.
(8) Department of Clinical Surgery, Royal Infirmary of Edinburgh, Edinburgh, UK.
(9) Department of Physiology, Development and Neuroscience, University of Cambridge, Cambridge, UK.
# equal contribution
*correspondence: m.huch@gurdon.cam.ac.uk

Abstract

Human liver cancer research currently lacks *in vitro* models that faithfully recapitulate the pathophysiology of the original tumour. We recently described a novel, near-physiological organoid culture system, where primary human healthy liver cells form long-term expanding organoids that retain liver tissue function and genetic stability. Here, we extend this culture system to the propagation of primary liver cancer (PLC) organoids from three of the most common PLC subtypes: hepatocellular carcinoma (HCC), cholangiocarcinoma (CC) and combined HCC/CC (CHC) tumours. PLC-derived organoid cultures preserve the histological architecture, gene expression and genomic landscape of the original tumour, allowing discrimination between different tumour tissues and subtypes, even after long term expansion in culture in the same medium conditions. Xenograft studies demonstrate that the tumourogenic potential, histological features and metastatic properties of PLC-derived organoids are preserved *in vivo*. PLC-derived organoids are amenable for biomarker identification and drug screening testing and lead to the identification of the ERK inhibitor SCH772984 as a potential therapeutic agent for primary liver cancer. We thus demonstrate the wide-ranging biomedical utilities of PLC-derived organoid models in furthering the understanding of liver cancer biology and in developing personalized medicine approaches for the disease.

Primary liver cancer (PLC) is the second most lethal malignancy worldwide, with incidence rates rising, mainly due to an increase in associated risk factors like diabetes or obesity[1,2]. The majority of all PLC are classified into either hepatocellular carcinoma (HCC) or cholangiocarcinoma (CC)[3]. There is also a combined hepatocellular-cholangiocarcinoma (CHC) subtype, which accounts for 0.4 to 14.2% of all PLCs[4]. Albeit HCC and CC are easily distinguishable by their histological appearance[2,5], genetic and transcriptional landscapes[6], with CHC sharing features of both[7], PLC is overall a complex entity, which renders each case of the disease unique and in need of personalized treatment.

The development of effective treatments for liver cancer has been hindered by the shortage of reproducible human models to assess the efficacy of candidate therapeutic agents[8]. Historically, preclinical models have mainly consisted of genetically engineered mouse models or human tumour-derived cell lines propagated in either 2D-culture or as xenografts in mice[8-10]. While 2D-culture has allowed pioneering advances in cancer biology, it fails to recapitulate critical features of a growing tumour *in vivo*[11], specially the 3D organization. In addition, CCs have proven difficult to propagate *in vitro*[12,13].

Recent reports of culture systems of primary, non-transformed tissues growing as 3D structures, termed organoids, accurately recapitulate tissue architecture and function. Thus retinal, cerebral, kidney, intestinal and stomach organoids (among others)[14] have already been generated from pluripotent stem cells for the study of human development and disease. In addition, organoids are promising disease models not only for understanding the biology but also for testing drug efficacy *in vitro*, before moving to animal models[15]. Accordingly, mouse and human cancer organoids have recently been established for colon[16-19], pancreas[17,20] and prostate[21] tumours, but not, thus far, from liver tumours.

Based on our previous work in mouse liver and pancreas organoid cultures[22-23], we recently showed that organoid cultures derived from human liver donor/healthy tissues could be expanded long-term *in vitro* while preserving most of their liver functionality and genetic stability over time[24]. Here, we demonstrate the proof-of-concept that liver organoid cultures also recapitulate human primary liver cancer *in vitro*. Hence, we have successfully established organoid cultures from 8 PLC patients, encompassing three of the most common subtypes of PLC[3]: HCC, CC and CHC. PLC-derived organoids recapitulate the histological architecture, expression profile, genomic landscape and *in vivo* tumourigenesis of the parental tumour, even after long-term expansion in culture. In addition, we demonstrate the utility of PLC-derived organoids for identifying genes with prognostic value for PLC and potential novel therapeutic targets, thus opening up opportunities for drug testing and advances in personalized medicine approaches.

RESULTS

Liver cancer organoids maintain the features of the parental tumour after long-term *in vitro* expansion.

We have recently established culture conditions for the long-term expansion of human cells derived from liver donor/healthy tissues[24,25]. Here, we sought to selectively expand tumour cells from human PLC tissue by optimizing our established human liver expansion protocol. Surgically resected liver tumour tissue was obtained from untreated PLC patients who had no history of viral-meditated hepatitis. Specimens (~1cm^3 tissue) from the 3 main PLC subtypes were obtained and each individual sample was split into 4 parts that were either processed for organoid derivation, histological diagnostic, genomic or transcriptomic analyses (Fig. 1a-b). We observed that normal/healthy contaminating tissue within the samples gave rise to organoids that would quickly outcompete the tumour-derived organoids, presumably due to differences in genetic stability, as previously suggested[19]. Therefore, to avoid the growth of healthy contaminating organoids, we modified our derivation protocol by (i) increasing the timing of tissue digestion, which reduced the yield of healthy contaminants; (ii) changing the starting culture conditions using, in addition of the classical isolation medium[24,25], a newly defined PLC-derived organoids isolation medium consisting in the classical isolation medium[24,25] without R-spondin-1, Noggin and Wnt3a but supplemented with Dexamethasone and Rho-kinase inhibitor for at least 2 weeks (Fig. 1c) and (iii) closely monitoring the developing organoid structures. Particularly, for all the samples in the manuscript we cultured half of the cell suspension in classical isolation medium and the other half in our tumouroid specific isolation medium, to ensure growth of the cultures (Supplementary Fig. 1 & methods). At the first passage all cultures (healthy and tumour, irrespective of their subtype-of-origin) were transferred to our previously defined "human healthy liver-derived organoids expansion medium"[24,25] and expanded and maintained in this medium.

Using this novel protocol, we successfully established human PLC-derived organoids from 8 different PLC patients, including poorly differentiated to moderate/well differentiated HCC (n=3) and CC (n=3), and combined HCC/CC (CHC; n=2) (Fig. 1, Supplementary Fig. 2a and Supplementary Table 1). We found a strong correlation between the derivation success rate (establishment) and the proliferation index of the original tumour. Thus, the efficiency of establishment of organoid cultures was 100% for those samples derived from tumours that contained > 5% proliferating cells (n=3 for HCC; n=2 for CHC and n=3 for CC), while we did not succeed in deriving organoids from very well differentiated lesions, with <5% proliferative cells in the original samples (n=8 for HCC and n=1 for CC), in agreement with the histological grading of early HCCs[5] (Supplementary Fig. 2b-g and Supplementary Table 1).

PLC-derived organoids (termed "tumouroids" henceforth) from all 3 different subtypes expanded long-term (~1year) in culture, with a consistent passaging ratio of 1:3-1:4 every 7-10 days. HCC-2, though, stopped growing after ~1 month, due to fibroblasts outcompeting the tumouroids growth, which precluded any downstream analysis. Therefore, we have performed all the downstream analysis on the remaining 7 lines and corresponding patient's tissues (HCC-1 and -3; CHC-1-2 and CC-1-3) (Fig. 1d and Supplementary Fig. 2h).

At the histological level, tumouroids presented patient-specific heterogeneous morphologies ranging from solid/compact structures (HCC and CHC) to more irregularly-shaped cyst-like structures (CC) in contrast to the ordered, homogeneous, cyst-like hollow structure of healthy liver-derived organoids (Fig. 1b and SupplementaryFig. 2a). These morphological features

allowed individual samples to be distinguished from each other, both within and between subtypes, even at late passage and after having been cultured for months in the same conditions.

We then sought to determine whether the 3D-tumouroids would retain the histological features of the patient tumour tissue. Healthy liver-derived organoids form single-layered epithelial structures that transition into a pseudo-stratified epithelium upon differentiation (see ref 24 for details). In contrast, the tumouroids exhibited a very different histological and cellular architecture, which recapitulated the histological features of the patient's tissue and tumour subtype. Thus, HCC and CHC tumouroids exhibited a solid, filled 3D structure with HCCs, but not CHCs, also forming pseudoglandular rosettes, typical of HCC[3,7]. Similarly, CC tumouroids exhibited extensive glandular domains with carcinoma cells invading the lumen and growing in cribriform structures, as observed in the patient's tissue (Fig. 1b and Supplementary Fig. 2a).

Detailed histological and marker analysis of all the patient's tumour tissues revealed that our cultures derived from a moderate/well differentiated HCC (HCC-1; AFP+/HepPar1+), a poorly differentiated HCC (HCC-3; AFP+/HepPar1-), a classical combined (CHC-1; AFP±/HepPar1+/EpCAM+/mucin+), a combined with stem cell features (CHC-2; AFP+/HepPar1+/EpCAM+/mucin-) and poorly to moderate/well differentiated CCs (CC-1-3; HepPar1-/EpCAM+) (Fig. 2a-b, Supplementary Fig. 3a-c and Supplementary Table 1)[26]. Subsequent analysis of these subtype-specific markers in the tumouroids revealed that these express the diagnostic markers of their parental tissues, even after long-term expansion in culture in the same culture conditions. Thus, EpCAM, was highly expressed in all CCs (CC-1-3) and CHCs (CHC-1-2) tumouroids and corresponding patients' tissues, but absent on HCCs tumouroids and tissues (Fig. 2c and Supplementary Fig.3b). Likewise, AFP a well-established marker for HCCs and a subset of CHCs[27], but not expressed in CCs[3,5,28-29], was highly expressed in both HCCs and CHC-2 tumouroids, in agreement with the expression pattern of the original patient's tissue (Fig. 2c and Supplementary Table 1). Remarkably, *SALL4* described for a subset of poorly differentiated HCCs[30-31] and CHCs[32] was only present in HCC-3 and CHC-2, both in tumouroids and matching tissues (Supplementary Fig. 3d).

Overall, these results demonstrate that liver tumouroids both recapitulated and retained the histological characteristics and marker expression of the original tumour tissue and subtype, even after long-term expansion in culture, in the same culture conditions.

Primary Liver Cancer-derived organoid cultures recapitulate the expression profile of the corresponding tissue-of-origin and tumour subtype.

The gene expression patterns of PLC subtypes (HCC, CC and CHC) have been extensively studied[33-34]. Therefore, to further characterize our tumouroid cultures we compared their expression profiles to the corresponding parental tissues using genome-wide transcriptomic (RNAseq) analysis. Healthy liver-derived organoid lines and corresponding tissues were used as additional controls.

Relative transcript abundance (transcripts per million, RPKM) of 15,648 gene transcripts was determined. Principal component analysis (PCA) analysis indicated that both technical and biological replicates per patient were almost identical (Supplementary Fig. 4a-b and Supplementary Dataset 1). Therefore, we present the data per patient as average of all these replicates. A first hierarchical clustering analysis comparing the gene expression profiles of our tissue samples with publically available TCGA PLC cohorts (344 HCC and 31 CC

samples) confirmed that the samples used in this study are representative of the overall population of primary liver cancer (Supplementary Fig. 4c and Supplementary Dataset 1). Then, we compared the expression profiles of these parental tissues to the corresponding tumouroid lines. Gene expression correlation analysis indicated that each tumouroid line correlated to its corresponding tissue-of-origin but not with the other subtypes (Fig. 3a). Along the same line, organoids and tissue samples grouped by subtype on the PC2 component, while the PC1 component accounted for the variance between tissues and tumour-derived organoids. Classical HCC/hepatocyte markers[35] such as *AFP* or *APOH* and CC/ductal markers[36] such as *KRT7*, were amongst the genes that contributed the most to the variance in the PC2 component (Fig. 3b and Supplementary Dataset 1).
When evaluating specific tumoural/differentiation markers, we found that the tumouroids' expression profiles resembled the corresponding matching tissues and subtype (Supplementary Fig 4d). Notably, we found the HCC markers (*AFP* and *GPC3)* and hepatocyte markers (*ALB, TTR, APOA1, APOE*) to be highly expressed in our HCC tumouroids and matching tissue while CC/ductal markers were amongst the most downregulated. Reciprocally, CC markers such as *EPCAM*, *KRT19* or *S100A11*[2,37,38-39] were highly expressed in our CC lines and tissues, while HCC markers were not expressed or strongly downregulated. The CHC lines shared the expression pattern of both, as expected (Fig. 2b-c, Fig. 3b-c, Supplementary Fig. 3b, Supplementary Fig. 4d and Supplementary Fig. 5a-b), and Supplementary Dataset 1). Remarkably, the expression pattern was also retained in a patient-specific manner even within each subtype. For instance, *MUC5B* was expressed only in CHC-1 but not in CHC-2 organoids, in agreement with the corresponding patient's tissue (Supplementary Dataset 1 and Supplementary Fig. 3c), whereas AFP was expressed in CHC-2 but not CHC-1 in concordance with the AFP values in serum of these patients at the moment of resection (compare Fig. 2c and Supplementary Table 1).

These results were confirmed by global analysis using Gene-Set-Enrichment-Analysis (GSEA) of the tumouroid lines and their corresponding parental tissues against 159 published cancer gene-sets (Fig. 3d and Supplementary Datasets 2 and 3). Thus, for both HCC lines and corresponding tissues, HCC gene-sets were the most significantly positively enriched, with HCC-1 associated to gene-sets describing HCC with hepatocyte differentiation features while HCC-3 significantly associated with a proliferative HCC subclass and a KRT19 positive subclass gene-sets in agreement with the differentiation status of the patient's original tissue. Conversely, for all CC tumouroids and matching tissues, CC gene-sets were the most significantly positively enriched whereas HCC specific gene-sets were significantly down-regulated, as expected. Similarly, the CHC expression profiles were negatively correlated with HCC-differentiation gene-sets but positively correlated with progenitor/stem cell, proliferation and/or poor prognosis gene-sets (Fig. 3d, Supplementary Fig. 5c-d and Supplementary Dataset 2 and 3).

Subsequent analyses confirmed the RNAseq results, with HCC but not CC tumouroids exhibiting hepatocyte differentiation features (ALB and HNF4a expression, Albumin secretion, and production of bile acid in the medium (the later for HCC-1)) (Supplementary Fig. 5b, e-f). In contrast, KRT19, marker for CC, CHC tumours[2,27] and a subset of HCCs[26], was highly expressed in all CC (CC-1-3), in both CHC (CHC-1-2) and in HCC-3 derived tumouroids, but undetectable in HCC-1, in agreement with the histological subtype, expression pattern and gene signature of the patient's tumour tissue (Supplementary Fig. 5a-b and d). Moreover, *KRT7*, a well-established marker for CCs[37], was only expressed in the CC-

derived organoids and corresponding tissues (Supplementary Fig. 5f).

These results demonstrate that the PLC-derived organoid culture system faithfully recapitulates and maintains the transcriptomic alterations present in the individual patient's tumour subtype. Since the different tumour subtypes were all maintained in the same culture conditions these results suggest that their tumour signature is intrinsic to the cancer population, and is not significantly modified by the culture conditions.

Tumouroid/Organoid cultures enable the identification of potential prognostic biomarkers for primary liver cancer

We next sought to investigate if the tumouroid culture system could represent a valuable resource to identify novel genes involved in PLC and/or novel potential PLC biomarkers, a use not previously described for any patient-derived organoid system. For that, we defined a "tumouroid signature" list by comparing the similarities between the transcriptomes of all tumouroid lines to healthy liver-derived organoid lines. Notably, within the top 30 most upregulated genes we found 19 genes already reported to be markers/overexpressed in PLC, 13 of which were already associated to poor-prognosis, while the remaining 11 genes had never been associated to PLC (Fig. 3e and Supplementary Dataset 1).

We then performed an in-depth analysis of these top 30 genes by determining their expression pattern and prognostic value in cohorts of primary liver cancer patients and healthy individuals from publically available TCGA databases (for HCC: 374 HCC patients and 50 healthy individuals; for CC: 31 CC patients and 8 healthy individuals). Notably, 29 of the top 30 genes were significantly ($p \leq 0.01$) overexpressed in cancer patients *vs* healthy individuals for both cohorts. Importantly, from the 11 novel genes never associated before to liver cancer, 4 exhibited poor survival prognosis when overexpressed: *C19ORF48, UBE2S* and *DTYMK* (for HCC) and *C1QBP* (for CC). Of note, *STMN1*, previously associated to HCC but not CC[40], also predicted poor survival in the CC-cohort (Fig. 3f-h and Supplementary Dataset 1). Therefore, these results demonstrate that growing primary liver cancer as tumouroids preserves the tumour-cell features at a level that allows identifying new genes with a prognostic value and that could potentially be used as prognostic biomarkers for primary liver cancer.

Liver tumouroids retain the genetic alterations present in the original tumour tissue.

PLCs typically present with a high degree of aneuploidy, several copy number changes, somatic mutations and epigenetic alterations[6]. All the lines that we expanded in culture (HCC, n=2; CHC, n=2; CC, n=3) exhibited multiple chromosomal aberrations consisting of both gains and/or losses of chromosome numbers (Fig. 4a-b). This was in stark contrast to healthy liver-derived organoids that stably maintained diploid chromosome numbers in culture, in agreement with our previous observations[24,41]. To determine whether the different tumouroid lines retain the parent tumour's mutational landscape, we performed whole exome sequencing (WES) analysis of each line expanded for short (<2 months, early passage) or extended (>4 months, late passage) periods in culture and compared the results to the corresponding parent tumour.

We generated ~19 Gb exome DNA sequence data from each sample. When comparing the global variant profile, we observed that, on average, ~92% of the variants in the patient's tissue were retained in the corresponding early tumouroid cultures (<2months), and >80%

even after months of expansion (Fig. 4c). Similarly, the analysis of the proportion of exonic variations for both patient's tissue and corresponding cultures confirmed that both, single nucleotide variants (SNVs) and Indels in the original tissue, are well retained in culture. Also, the distribution of base substitutions for both tissues and tumouroids revealed an over-representation of the T>C/A>G and C>T/G>A transversion, in agreement with the mutational spectrum described for CCs and HCCs[42-43] (Fig. 4d-e). Of note, we did not find significant bias between transcribed and untranscribed strands (Supplementary Fig. 6a).
Since we lacked matched germline (normal/non-tumour) mutational data, in order to select for cancer related variants we filtered for variants present in COSMIC and excluded polymorphisms by using publically available databases following the guidelines described in ref 44 (see methods). The majority of all the cancer-related somatic variants present in the patient's original tissue were retained in the corresponding tumouroid cultures (~84%). In fact, <16% (in average) were lost between tissue and early tumouroids, thus suggesting that the cultures represent the tumour genetic landscape of the original patient, with little bias of tumouroids cells harbouring specific mutations (~0.5 % in average) (Fig. 4f). The total number of deleterious mutations that could impact protein function ranges from 70 to 294, in agreement with published mutational burdens for HCC and CC tumours[42,45] (Supplementary Fig. 6b, Supplementary Dataset 4).

Next-generation sequencing studies have created a detailed map of the genetic alterations present in liver cancer and its subtypes[6]. In agreement with this mutational spectrum, HCC-1 line and corresponding patient tissue exhibited missense mutations in *CTNNB1* (Fig. 4g and Supplementary Dataset 4), consistently with their significant enrichment in CTNNB1 mutated liver cancer gene-set found in the gene GSEA (Fig. 3d) and their elevated levels of Wnt target genes (Supplementary Dataset 1). CHC-2 line harboured a *TP53* frameshift variant (L206fs). Also, we identified an activating mutation in *KRAS* (*KRASG12D*) in CC-1 and CHC-1 tumouroid lines and matching tissues, but not in the HCC lines, in agreement with the significant enrichment in EGF activated gene-set for those lines (Supplementary Fig. 6c)[46]. We also found nonsense mutations and a disruptive deletion in the chromatin remodelling genes *ARID1A* (HCC-3 and CC-1) and *ARID2* (HCC-3), in agreement with previous reports where both genes are altered in all subtypes of PLC[47-48] (Fig. 4g, and Supplementary Dataset 4). As expected, all lines were devoid of mutations in *MAPK1* and *MAPK3* (ERK1 and ERK2 respectively), as described for PLC[45].

Therefore, these results indicate that the PLC tumouroid culture system retained the mutational landscape of the original tumour tissue and faithfully retained the tumour subtype specific mutations present in the original sample from which where derived.

Tumouroids recapitulate the histology of the parental tumour and show metastatic potential *in vivo*

To determine whether tumouroids also recapitulate the features of a human primary liver tumour *in vivo*, we transplanted CC (CC-1-3 lines) and HCC-1 long-term expanded tumouroids under the skin of immunocompromised mice. Healthy liver-derived organoids were used as controls (Fig. 5a). We found tumour outgrowths in the animals engrafted with CC-1_O (29/29), CC-2_O (8/8) and HCC-1_O (24/34), but not when injected with healthy liver-derived organoids (Healthy-1_O) (Fig. 5b and Supplementary Fig. 7a-b). The CC-derived tumours exhibited a strong stromal reaction with CC-1_O tumours forming glands with proliferative cells growing in cribriform structures (Fig. 5c Supplementary Fig. 7c, and

CC-2_O exhibiting a more differentiated phenotype (Supplementary Fig. 7 d), reminiscent of the corresponding patient's tumour tissue. Similarly, HCC-1_O derived tumours grew as a solid mass with proliferative cells (Supplementary Fig. 7c) and exhibited pseudoglandular rosettes, as in the patient's tissue (Fig. 5d). Secondary tumouroids derived from these xenografted tumours exhibited similar chromosome counts and were morphologically and histologically indistinguishable from their parental line (Supplementary Fig. 7e-f). Hence, this indicated that even after long-term expansion *in vitro* and transplantation *in vivo*, expanding primary liver tumours in organoid culture, stably preserves the histological architecture of the parent tumour.

Primary liver cancer has been reported to metastasize primarily to the lung and portal lymph nodes[49]. To determine whether our tumouroid models would faithfully recapitulate liver cancer metastatic phenotype, we injected CC-1_O, derived from a patient with history of metastasis, into the kidney capsule of NSG mice. As expected, 100% of the injected mice developed tumours that resembled the original patient tissue (Fig. 5b and e). More importantly, in 7 out of 9 injected mice we found lung metastases, in agreement with the patient's diagnostic at the moment of resection (Supplementary Table 1), while, as expected, healthy liver-derived organoids (Healthy-1_O) did not generate any metastases (Fig. 5b and f, Supplementary Fig. 7 g-h)

Overall, these results establish that primary liver cancer-derived organoids accurately model the histological and metastatic features of their parent tumours *in vivo,* even after long-term expansion in culture.

Liver tumouroids allow the identification of patient-specific drug sensitivities and uncover ERK as a potential target for primary liver cancer

We performed proof-of-concept drug sensitivity testing in 6 of the PLC tumouroids lines (HCC-1; HCC-3; CHC-1,-2; CC-1,-2) to evaluate their use to identify patient-specific sensitivities and as a platform to inform drug development. As an initial prioritization step, for each tumouroid line we tested their sensitivity to 29 anti-cancer compounds, including drugs in clinical use or development. Tumouroids were treated with a dilution series of each compound for 6 days, before measuring cell viability[50]. Drug sensitivity was represented by the area under the dose response curve (AUC) and by the half-maximal inhibitory concentration (IC_{50}) (Fig. 6a-c and Supplementary Dataset 5). The assay was conducted with technical replicates and two biological replicates per tumouroid were independently screened. There was a positive correlation of biological AUC replicates (R_p = 0.79) and IC_{50} replicates (R_p = 0.73) across the dataset. CC-2 was insensitive to all compounds and so was excluded from further analyses.

From our initial prioritization screen, we confirmed drug sensitivity for a subset of compounds using a tumouroid formation assay, thus validating our screening method. We selected clinically relevant compounds where differential sensitivity was observed across the tumouroid panel; namely Taselisib, Gemcitabine, AZD8931, SCH772984 and Dasatanib (Fig. 6c-d). Overall, a good agreement between the screening and validation results was observed (Supplementary Fig. 8a). For instance, Taselisib resulted in a growth inhibitory effect in 5 of 6 tumouroids while Dasatinib suppressed tumouroid formation only in CC-1 cells, both results in agreement with our screening results. An exception was for CC-1 line with AZD8931, where we observed a variable sensitivity between biological replicates in the prioritization screen (Fig. 6 c-d, Supplementary Fig. 8a).

Overall, tumouroids were resistant to the majority of the compounds, with an IC_{50} greater than the maximum screening concentration, although we detected interesting sensitivity to several compounds demonstrating a correlation between some drug sensitivities and mutational profiles in the tumouroid lines. For instance, HCC-1 harbouring mutations in *CTNNB1* gene, was resistant to the porcupine inhibitor LGK974, whereas CC-1, Wnt-dependant tumour (Fig.1c), was sensitive (Fig. 6a-c). Moreover, EGFR-family inhibition with AZD8931 restricted tumouroid formation in HCC-1 cells (wild-type for *KRAS*), whereas the other lines, and notably CC-1 and CHC-1 (*KRAS* mutants) were resistant. Interestingly we also observed tumouroid sensitivity to Gemcitabine, which is used clinically for the treatment of PLC patients (Fig. 6a-c).

Of particular interest was the substantial inhibition of tumouroid formation following inhibition of ERK1/2 by SCH772984 in HCC1-3, CC-1 and CHC-1 cells (Fig. 6a-d and Supplementary Fig. 8a). SCH772984, which selectively inhibited ERK-phosphorylation in HCC-1 and CC-1 tumouroids (Supplementary Fig. 8b), was effective in lines that were insensitive to the BRAF and/or MEK inhibitors in our screen (Dabrafenib and Trametinib) (Fig. 6c). The reason for this difference is unclear, although ERK inhibitors have demonstrated activity in cells with acquired BRAF and MEK inhibitor-resistance[51].
We note that clinical trials exploring the effect of specific ERK inhibitors for PLC have not been reported thus far. Hence, to further investigate the potential of ERK1/2 inhibition for PLC, we tested the efficacy of SCH772984 to inhibit tumour growth *in vivo*. For that, CC-1 and HCC-1-derived tumouroids were transplanted subcutaneously into NSG mice and, when tumours reached ~100mm^3, those were injected intra-tumourally with either SCH772984 or the vehicle. Remarkably, 2-7 days after the first injection we observed a significant reduction in tumour growth, which lasted for the remainder of the experiment (Fig. 6e and Supplementary Fig. 8c). Histological analysis revealed that the tumour mass was necrotic and that the majority of the cells were apoptotic (Fig. 6f-g and Supplementary Fig. 8d). Western blot analysis confirmed that SCH772984 also *in vivo* selectively inhibited ERK-phosphorylation in CC-1 tumours (Supplementary Fig. 8e). Thus, in aggregate, our proof-of-concept study demonstrates the application of PLC tumouroids for *in vitro* and *in vivo* drug testing, and provides initial evidence that ERK inhibition could have a beneficial therapeutic effect on a subset of HCC and CC patients.

Overall, these results indicate that by faithfully retaining the histological, transcriptomic and genomic landscape of their parent tumour, tumouroid cultures facilitate the prediction of drug sensitivity/resistance in a patient-specific manner. Therefore, they provide an important new resource for liver cancer research, opening up new avenues for biomarker discovery and drug testing.

DISCUSSION

The advent of 3D culture systems has made it possible to partially recapitulate the complexity and function of mammalian tissue *in vitro*, by forming structures that resemble an adult organ in culture and which have been termed "organoids"[14]. We recently have demonstrated that gastric, pancreatic and hepatic organoid cultures derived from adult tissues self-renew and differentiate *in vitro*, into the corresponding cell types of the tissue-of–origin[14-15].

Here, we demonstrate the proof-of-concept that primary liver cancer (PLC) tissue grown as organoid cultures (here termed tumouroid) faithfully models the genetic complexity of human PLC *in vitro*. We successfully established cultures from tumours derived from 8 PLC patients representing the three most common subtypes of PLC[3]: HCC, CC and CHC. In contrast to any liver cancer cell line grown in 2D, PLC-derived organoids recapitulate the histological architecture and expression profiles of the corresponding parent tumour, even after long-term expansion in the same culture conditions for all subtypes or upon transplantation into mice. Notably, they also retain the specific differences between patients as well as between tumour subtypes. We have exploited this aspect here to demonstrate the proof-of-concept that tumour-derived organoid cultures could represent a valuable resource for biomarker discovery, especially for prognostic markers, an application not previously reported for any organoid culture system. We report *C19ORF48, UBE2S, DTYMK* (for HCC) and *C1QBP* and *STMN1* (for CC) as all novel genes associated to poor prognosis for primary liver cancer. Further studies, though, will be necessary to prove their utility as prognostic or their relevance as predictive biomarkers and/or their potential direct involvement in the progression of the disease. These results open up novel opportunities in using tumour-derived organoids for tumour marker discovery.

A unique and important feature of the tumouroids is that they maintain the mutational landscape of the original patient's tumour, even after long-term expansion in culture. This is vastly different to existing 2D cell lines, which albeit they cover the major driver mutations observed in many cancer sub-types[52], no longer present the patient-specific signature and genetic landscape of the original tumours from whence they were derived, exemplified by the frequent acquisition of mutations in *TP53* in such cell lines[53]. The reasons for these differences are unknown, but it is feasible to speculate that the cell-matrix interactions may play an important role. In fact, embedding primary tumoural epithelial cells within an extracellular matrix (ECM) enables the cells to interpret the environment and self-assemble into structures which acquire tissue patterning, as it occurs during development and organogenesis. Also, the cell-matrix interactions established in 3D could prevent anoikis-apoptosis due to detachment from the matrix[54]- of those tumoural cells that have not acquired yet all the mutations to survive in a ECM-free milieu, thus facilitating the maintenance of heterogeneous, non-selected populations within the culture. In that line, our results indicate that if selection of specific tumoural cells exist in the cultures, this might have a minor effect at the population level, as we found that tumouroids harbour >92% of the SNVs present in the original tissue.

The reproduction of parent tumour genetic aberrations in a culture setting makes tumouroid lines a potentially valuable resource in screening drug sensitivity/resistance, identifying novel players in primary liver cancer, or even novel therapeutics as part of a personalized medicine approach. Our results validate such an approach by (1) demonstrating a correlation between

some drug sensitivities and the mutational profile in the tumouroid lines and (2) the *de novo* identification of the ERK inhibitor SCH772984 as a potential novel therapeutic agent for PLC. Future studies aiming at validating the efficacy of ERK inhibition in a bigger collection of tumouroid lines will be required, though, to confirm its therapeutic value for liver cancer.

The lack of immune system and stromal components, though, represents a limitation of the culture system, especially when aiming at studying tumour cell-stroma/immune interactions. In that regard, patient derived xenografts (PDXs) have proven useful models for human cancer, including liver cancer[13,55], as they also retain tumour histopathology, including tumour-infiltrating lymphocytes and the stromal component, and global gene expression and methylation profiles of the patient's malignant epithelial cells[56]. However, PDXs suffer from a low engraftment rate, especially CCs (5.8% engraftment efficiency as reported by Cavalloni et al.,[13]), have a long engraftment period (often several months), are expensive and time-consuming, and are not tractable for large-scale drug sensitivity testing[56]. Therefore, we believe that the PLC-derived organoid cultures we present here are complementary and alternative models to liver cancer PDXs. Furthermore, they are suitable for large-scale drug testing, and in a timescale that makes it potentially compatible with personalized medicine approaches.

In conclusion, the PLC-derived organoids that we present here fulfil all the criteria of a reliable *in vitro* cancer model, recapitulating all the features of three of the most common subtypes of liver tumours, from histological architecture to genetic and transcriptomic traits, and are amenable as a platform for drug screening. With a short timescale from establishment to drug testing, this novel *in vitro* primary liver cancer system thus makes hitherto inaccessible possibilities for predicting patient-specific drug responses and creating personalized/*à la carte* therapies into a reality.

ACKNOWLEDGEMENTS

M.H. is a Wellcome Trust Sir Henry Dale Fellow and is jointly funded by the Wellcome Trust and the Royal Society (104151/Z/14/Z). L.B. is supported by an EMBO Postdoctoral fellowship (EMBO ALTF 794-2014) and Marie-Curie Postdoctoral fellowship (Grant 656193_H2020-MSCA-IF-2014). G.M. was supported by a Marie Curie Initial Training Network (Marie Curie ITN WntsApp 608180) and a H2020 LSMF4LIFE grant (ECH2020-668350). This work was funded by an NC3Rs International prize, a Beit Prize, a Cambridge Cancer Center-pump priming award (CRUK-RG83267) and, partially, by a NC3Rs project grant (NC/R001162/1), all of them awarded to M.H. Work at the L.J.W.v.d.L lab was funded by the research program InnoSysTox, [project number 114027003], by the Netherlands Organisation for Health Research and Development (ZonMw) and part of the research program financed by the Dutch Digestive Foundation [MLDS-Diagnostics project number D16-26]. Work in the MJG lab is funded by the Wellcome Trust (102696), Stand Up To Cancer (SU2C-AACRDT1213), and Cancer Research UK (C44943/A22536).

We thank Dr Clare Pacini for help with the clustering analysis of the HCC and CC TCGA-cohorts and the samples used in this study. We also thank Ms Cora Olpe and Mr Nicholas Hircq for help in the early phases of the project, Dr Chris Hindley for editorial assistance, The Gurdon Institute facilities for help with imaging and animal care, Dr. Sylviane Moss, Dr Maike Paramor and Dr Joaquin Martinez for assistance with sequencing analysis and Dr Asif Jah (Cambridge University Hospitals NHS Trust) and Dr Jeroen de Jonge (Erasmus Rotterdam Center) for facilitating recruitment of patients. Finally, M.H. would like to thank Prof Brigid Hogan (Chapel Hill) and Prof Magdalena Zernicka-Goetz (University of Cambridge) for helpful discussions and critical comments.

AUTHOR CONTRIBUTIONS

L.B., designed and performed experiments and interpreted results. G.M., performed experiments and interpreted results. R.A-B. and O.S. performed experiments. L.M.G., C.R.B., G.E.A. and S.D. performed bioinformatic analyses. S.E.D., performed the histopathology diagnosis. M.M.A.V., M.P.G, R.L., J.N.M.I.J., S.J.W, R.K.P., N.G. and K.S.P., provided patient material and interpreted clinical data. K.S.P., performed the kidney capsule transplants. H.E.F. and M.J.G. performed the drug screening, interpreted the results and wrote this section of the manuscript. M.H. conceived and designed the project, designed and performed experiments and interpreted results. M.H. and L.B. wrote the manuscript. All authors commented on the manuscript.

COMPETING FINANCIAL INTERESTS

The authors declare no competing financial interests.

REFERENCES

1. Bosch, F.X., Ribes, J., Díaz, M. & Cléries, R. Primary liver cancer: Worldwide incidence and trends. *Gastroenterology* **127**, S5-S16 (2004).
2. Bridgewater, J.*, et al.* Guidelines for the diagnosis and management of intrahepatic cholangiocarcinoma. *Journal of Hepatology* **60**, 1268-1289 (2014).
3. Hirohashi, S.*, et al.* Tumours of the Liver and Intrahepatic Bile Ducts. in *World Health Organization Classification of Tumours* (eds. Stanley R. Hamilton, M.D. & Lauri A. Aaltonen, M.D., Ph.D.) (IARCPress, 69372 Lyon, France, 2000).
4. Lee, S.D.*, et al.* Clinicopathological features and prognosis of combined hepatocellular carcinoma and cholangiocarcinoma after surgery. *Hepatobiliary Pancreat Dis Int* **13**, 594-601 (2014).
5. International Consensus Group for Hepatocellular, N. Pathologic diagnosis of early hepatocellular carcinoma: A report of the international consensus group for hepatocellular neoplasia. *Hepatology* **49**, 658-664 (2009).
6. Marquardt, J.U. & Andersen, J.B. Liver cancer oncogenomics: opportunities and dilemmas for clinical applications. *Hepatic oncology* **2**, 79-93 (2015).
7. Wang, A.-Q.*, et al.* Combined hepatocellular cholangiocarcinoma: Controversies to be addressed. *World Journal of Gastroenterology* **22**, 4459-4465 (2016).
8. Sharma, S.V., Haber, D.A. & Settleman, J. Cell line-based platforms to evaluate the therapeutic efficacy of candidate anticancer agents. *Nat Rev Cancer* **10**, 241-253 (2010).
9. De Minicis, S.*, et al.* Liver carcinogenesis: Rodent models of hepatocarcinoma and cholangiocarcinoma. *Digestive and Liver Disease* **45**, 450-459 (2013).
10. Oikawa, T.*, et al.* Model of fibrolamellar hepatocellular carcinomas reveals striking enrichment in cancer stem cells. *Nature Communications* **6**, 8070 (2015).
11. Shamir, E.R. & Ewald, A.J. Three-dimensional organotypic culture: experimental models of mammalian biology and disease. *Nature reviews Molecular cell biology* **15**, 647-664 (2014).
12. Ku, J.L.*, et al.* Establishment and characterisation of six human biliary tract cancer cell lines. *British Journal of Cancer* **87**, 187-193 (2002).
13. Cavalloni, G.*, et al.* Establishment and characterization of a human intrahepatic cholangiocarcinoma cell line derived from an Italian patient. *Tumour Biology* **37**, 4041-4052 (2016).
14. Huch, M. & Koo, B.-K. Modeling mouse and human development using organoid cultures. *Development* **142**, 3113-3125 (2015).
15. Hindley, C.J., Cordero-Espinoza, L. & Huch, M. Organoids from adult liver and pancreas: Stem cell biology and biomedical utility. *Developmental Biology*.
16. Crespo, M.*, et al.* Colonic organoids derived from human induced pluripotent stem cells for modeling colorectal cancer and drug testing. *Nat Med* **23**, 878-884 (2017).
17. Li, X.*, et al.* Oncogenic transformation of diverse gastrointestinal tissues in primary organoid culture. *Nature medicine* **20**, 769-777 (2014).
18. Sato, T.*, et al.* Long-term Expansion of Epithelial Organoids From Human Colon, Adenoma, Adenocarcinoma, and Barrett's Epithelium. *Gastroenterology* **141**, 1762-1772 (2011).

19. van de Wetering, M., *et al.* Prospective derivation of a living organoid biobank of colorectal cancer patients. *Cell* **161**, 933-945 (2015).
20. Boj, S.F., *et al.* Organoid Models of Human and Mouse Ductal Pancreatic Cancer. *Cell* **160**, 324-338 (2015).
21. Gao, D., *et al.* Organoid Cultures Derived from Patients with Advanced Prostate Cancer. *Cell* **159**, 176-187 (2014).
22. Huch, M., *et al.* Unlimited in vitro expansion of adult bi-potent pancreas progenitors through the Lgr5/R-spondin axis. *The EMBO Journal* **32**, 2708-2721 (2013).
23. Huch, M., *et al.* In vitro expansion of single Lgr5+ liver stem cells induced by Wnt-driven regeneration. *Nature* **494**, 247-250 (2013).
24. Huch, M., *et al.* Long-Term Culture of Genome-Stable Bipotent Stem Cells from Adult Human Liver. *Cell* **160**, 299-312 (2015).
25. Broutier, L., *et al.* Culture and establishment of self-renewing human and mouse adult liver and pancreas 3D organoids and their genetic manipulation. *Nat Protoc* **11**, 1724-1743 (2016).
26. Brunt, E.M.P., V.; Sempoux, C.; Theise, N.D. Biphenotypic (hepatobiliary) primary liver carcinomas: the work in progress. *Hepatic Oncology* **2**, 18 (2015).
27. Zhang, F., *et al.* Combined hepatocellular cholangiocarcinoma originating from hepatic progenitor cells: immunohistochemical and double-fluorescence immunostaining evidence. *Histopathology* **52**, 224-232 (2008).
28. Zhao, Y.-J., Ju, Q. & Li, G.-C. Tumor markers for hepatocellular carcinoma. *Molecular and Clinical Oncology* **1**, 593-598 (2013).
29. Ohguchi, S., *et al.* Expression of α-fetoprotein and albumin genes in human hepatocellular carcinomas: Limitations in the application of the genes for targeting human hepatocellular carcinoma in gene therapy. *Hepatology* **27**, 599-607 (1998).
30. Yakaboski, E., Jares, A. & Ma, Y. Stem cell gene SALL4 in aggressive hepatocellular carcinoma: a cancer stem cell-specific target? *Hepatology* **60**, 419-421 (2014).
31. Yong, K.J., *et al.* Oncofetal gene SALL4 in aggressive hepatocellular carcinoma. *N Engl J Med* **368**, 2266-2276 (2013).
32. Moeini, A., *et al.* Mixed hepatocellular cholangiocarcinoma tumors: Cholangiolocellular carcinoma is a distinct molecular entity. *J Hepatol* **66**, 952-961 (2017).
33. Shibata, T. & Aburatani, H. Exploration of liver cancer genomes. *Nature Reviews Gastroenterology & Hepatology* **11**, 340-349 (2014).
34. Woo, H.G., *et al.* Identification of a cholangiocarcinoma-like gene expression trait in hepatocellular carcinoma. *Cancer research* **70**, 3034-3041 (2010).
35. Kalinich, M., *et al.* An RNA-based signature enables high specificity detection of circulating tumor cells in hepatocellular carcinoma. *Proc Natl Acad Sci U S A* **114**, 1123-1128 (2017).
36. Kamlua, S., *et al.* A novel TFF2 splice variant (ΔEX2TFF2) correlates with longer overall survival time in cholangiocarcinoma. *Oncology Reports* **27**, 1207-1212 (2012).
37. Banales, J.M., *et al.* Expert consensus document: Cholangiocarcinoma: current knowledge and future perspectives consensus statement from the European Network for the Study of Cholangiocarcinoma (ENS-CCA). *Nat Rev Gastroenterol Hepatol* **13**, 261-280 (2016).

38. Kraiklang, R., *et al.* A novel predictive equation for potential diagnosis of cholangiocarcinoma. *PLoS One* **9**, e89337 (2014).
39. Andersen, J.B., *et al.* Genomic and genetic characterization of cholangiocarcinoma identifies therapeutic targets for tyrosine kinase inhibitors. *Gastroenterology* **142**, 1021-1031 e1015 (2012).
40. Hsieh, S.Y., *et al.* Stathmin1 overexpression associated with polyploidy, tumor-cell invasion, early recurrence, and poor prognosis in human hepatoma. *Mol Carcinog* **49**, 476-487 (2010).
41. Blokzijl, F., *et al.* Tissue-specific mutation accumulation in human adult stem cells during life. *Nature* **538**, 260-264 (2016).
42. Zou, S., *et al.* Mutational landscape of intrahepatic cholangiocarcinoma. *Nat Commun* **5**, 5696 (2014).
43. Totoki, Y., *et al.* High-resolution characterization of a hepatocellular carcinoma genome. *Nat Genet* **43**, 464-469 (2011).
44. Li, M.M., *et al.* Standards and Guidelines for the Interpretation and Reporting of Sequence Variants in Cancer: A Joint Consensus Recommendation of the Association for Molecular Pathology, American Society of Clinical Oncology, and College of American Pathologists. *J Mol Diagn* **19**, 4-23 (2017).
45. Schulze, K., *et al.* Exome sequencing of hepatocellular carcinomas identifies new mutational signatures and potential therapeutic targets. *Nat Genet* **47**, 505-511 (2015).
46. Borlak, J., Meier, T., Halter, R., Spanel, R. & Spanel-Borowski, K. Epidermal growth factor-induced hepatocellular carcinoma: gene expression profiles in precursor lesions, early stage and solitary tumours. *Oncogene* **24**, 1809-1819 (2005).
47. Jiao, Y., *et al.* Exome sequencing identifies frequent inactivating mutations in BAP1, ARID1A and PBRM1 in intrahepatic cholangiocarcinomas. *Nat Genet* **45**, 1470-1473 (2013).
48. Li, M., *et al.* Inactivating mutations of the chromatin remodeling gene ARID2 in hepatocellular carcinoma. *Nat Genet* **43**, 828-829 (2011).
49. Lee, Y.T. & Geer, D.A. Primary liver cancer: pattern of metastasis. *J Surg Oncol* **36**, 26-31 (1987).
50. Francies, H.E., Barthorpe, A., McLaren-Douglas, A., Barendt, W.J. & Garnett, M.J. Drug Sensitivity Assays of Human Cancer Organoid Cultures. *Methods Mol Biol* (2016).
51. Morris, E.J., *et al.* Discovery of a novel ERK inhibitor with activity in models of acquired resistance to BRAF and MEK inhibitors. *Cancer Discov* **3**, 742-750 (2013).
52. Iorio, F., *et al.* A Landscape of Pharmacogenomic Interactions in Cancer. *Cell* **166**, 740-754 (2016).
53. Drexler, H.G., *et al.* p53 alterations in human leukemia-lymphoma cell lines: in vitroartifact or prerequisite for cell immortalization? *Leukemia* **14**, 198-206 (2000).
54. Frisch, S.M., Schaller, M. & Cieply, B. Mechanisms that link the oncogenic epithelial–mesenchymal transition to suppression of anoikis. *Journal of Cell Science* **126**, 21-29 (2013).
55. Gu, Q., *et al.* Genomic characterization of a large panel of patient-derived hepatocellular carcinoma xenograft tumor models for preclinical development. *Oncotarget* **6**, 20160-20176 (2015).

674 56. Hidalgo, M., *et al.* Patient-derived xenograft models: an emerging platform for
675 translational cancer research. *Cancer Discov* **4**, 998-1013 (2014).
676

FIGURE LEGENDS

Figure 1: Patient-derived primary liver cancer organoid cultures expand long-term *in vitro* while preserving the histological architecture of the tumour subtype they derived from.

(a) Experimental design. Healthy (donor-derived) liver tissues, moderate/well differentiated hepatocellular carcinoma (HCC), combined hepatocellular-cholangiocarcinoma (CHC) and cholangiocarcinoma samples (CC) were obtained from patients undergoing surgery (patient's information detailed in Supplementary Table 1) and were processed as described in Methods and Supplementary Fig. 1. **(b)** Representative H&E staining of healthy liver tissue and primary tumours (top row), and corresponding brightfield microscopy images (middle row) and H&E histological analysis of the organoid lines derived from these (bottom row). Note that, while healthy liver-derived organoids (left) grew as single layered epithelium of ductal-like cells surrounding a central lumen (*, duct; L, lumen), tumour-derived organoids (tumouroids; right) formed compacted structures that resembled the corresponding tumour-of-origin. HCC-1 tumouroids, like their parental tissue, exhibit pseudoglandular rosettes (arrowheads), a hallmark of HCC. CC-1 tumouroids present a glandular lumen, similar to the patient's tumour (top row). Scale bars, middle row 100µm; top and bottom rows, 50µm. Brightfield and H&E pictures from other lines are provided in Supplementary Fig. 2. **(c)** Organoid formation efficiency in classical human healthy liver isolation medium[24-25] and tumouroid specific isolation medium (classical human healthy liver isolation medium without Rspo-1, Noggin and Wnt3a and 3nM Dexamethasone - see methods and Supplementary Fig. 1 for details). Graph represents the mean±SD of the organoid formation efficiency in tumouroid IM relative to the one in classical IM. Individual data points are shown (circle). Significant differences between the classical and tumouroid IM groups were observed. **, p-value<0.001 (t-test, two-tailed). **(d)** Expansion potential of tumouroid cultures established and their correlation to the expansion of healthy-tissue derived organoids. Arrow, continuous expansion. Dot, passage.

Figure 2: Immunohistochemistry analyses reveal that the PLC tumouroids retain expression patterns of the distinct subtype of the original tissue they derived from, even after long-term expansion in culture.

(a) Schematic representation of the multiple subtypes of primary liver cancers (PLC). **(b)** IHC assays on the PLC tissues including hepatocyte/HCC marker (HepPar1) and ductal/CC marker (EpCAM). Scale bar, 125 µm. Dashed red square indicates focal staining. **(c)** Immunofluorescent analysis for the HCC marker AFP (red) and the ductal/CC marker EpCAM (green), on tumouroids expanded in culture for at least 3 months. Nuclei were counterstained with Hoechst33342 (blue). Scale bar, 30µm.

Figure 3: Tumouroids recapitulate the expression profiles of the specific tissue of origin.

(a) Correlation heat map between PLC-tissue (_T) and paired PLC-derived organoid line (_O) expression profiles' after at least >2 months expansion in culture. **(b)** Principal component analysis (PCA) showing samples plotted in 2 dimensions using their projections onto the first two principal components (PC1 and PC2). Each data point represents one sample (circle, tumouroid; triangle, tissue). PC1 is strongly correlated with the type of sample (tumouroids vs tissue) whereas PC2 defines the 3 different PLC subtypes (HCC, red; CHC, brown; and CC, green). Representative examples from the top-100 genes with highest loadings across PC2 are shown. **(c)** Heat map analysis of the log2 RPKM values (raw z-scored) of selected genes found highly expressed (red) in HCC and/or CHC and/or CC tumouroids. Top left column indicates whether the indicated genes are markers of HCC/Hepatocyte/Fetal liver/CC/Ductal or liver progenitor markers. **(d)** Heat-map indicating representative gene-sets significantly (False discovery rate (FDR)<25%) UPregulated (purple) and DOWNregulated (green) in the

tumouroid lines and paired tissues after performing gene set enrichment analysis (GSEA) comparing their gene signatures to 159 curated gene-sets associated with liver cancer and stem cell (representative plots are shown in Supplementary Fig. 5). Full list of gene-sets and significantly enriched gene-sets can be found in Supplementary Dataset 2 and 3. **(e)** Schematic of the tumouroid signature. Venn diagram overlapping the upregulated genes in each tumouroid line compared to healthy organoids. **(f)** Table summarizing the results of the gene expression (OE, overexpression) and outcome prediction (KM, Kaplan-Meier) analyses for the top 25-genes of the tumouroid signature using publically available TCGA cohorts. The table details the p-values obtained (OE, two-sided t-test ; KM, log-rank test). Statistical significance (p-value≤0.05) is denoted by yellow color. Values for the top 30-genes can be found in Supplementary Dataset 1. TCGA-HCC, 374 tumour/50 normal samples; TCGA-CC, 31 tumour/8 normal samples. **(g)** Expression of *STMN1*, *C1QBP* and *C19orf48* in tumour and normal tissues in the TCGA-HCC and/or CC cohorts. Center line, median; box plot, interquartile range (IQR); whiskers, range (minimum to maximum). **(h)** Kaplan-Meier analyses of the TCGA-HCC and/or TCGA-CC cohorts based on the expression level of the indicated genes in the cohorts samples.

Figure 4: Tumouroids preserve the genetic alterations from the original tumour

(a) Ploidy analysis of tumouroid cultures expanded for at least 2 months in culture. Results are expressed as % of ploidy per number of metaphases counted (at least 21 total). Healthy-derived organoids were used as control. A minimum of two independent experiments were performed. **(b)** Representative images of organoid metaphases used for the ploidy analysis. Scale bar, 10µm. **(c-e)** Whole exome sequencing analysis of patient's tumour tissues and corresponding tumouroid cultures expanded for < 2 months (early passage) or >4 months (late passage) in culture. All variants identified in all samples (21 total; 7 patients with 3 samples each (Tissue/early organoid/late organoid) were used for the global analyses after filtering for quality control as detailed in methods). **(c)** Correlation heat-map between the variants identified in PLC-tissues (_T) and PLC-tumouroids (_O). **(d)** Proportions of exonic variants across the samples, the 6 types of SNVs and the Indels are represented. **(e)** Percentage of the 6 types of SNVs averaged across all samples. Graph represents mean±SD. **(f-g)** A cancer-related set of variants (f) and variants predicted to impair protein function (SIFT score <0.05 filter) (g) were identified as described in methods. **(f)** Bar plots indicate the concordance (%) between the cancer-related variants identified in the tumour-of-origin and the corresponding tumouroids expanded for short term in culture. **(g)** Damaging coding mutations found in genes already described mutated in liver cancer (Full list is found in Supplementary Dataset 4, spread sheet 15 details the references). The type of mutation is indicated in the legend. _T, tissue; _O, organoid.

Figure 5: *In vivo* growth and metastatic potential of PLC tumouroids

(a) Experimental design. PLC tumouroids or Healthy liver-derived organoids expanded for >3 months in culture were transplanted subcutaneously (SC) or under the kidney capsule (Kid.Cap.) of immunocompromised NSG mice and analysed for the presence of tumour growth and metastasis following grafting. **(b)** Tables summarizing the number of cells, site of engraftment and analysis of tumour and lung metastasis. No tumour lesions were found in any of the mice injected with Healthy-1 organoids. **(c-d)** Representative H&E staining of CC-1 (c) and HCC-1 (d) tumouroids transplanted subcutaneously (top) into NSG mice and corresponding patient's tumour sample (bottom). **(c)** Note that the grafted CC-1 tumouroid tissue (top) recapitulates the histo-architecture of the patient's original tumour (bottom)

including the extensive desmoplastic reaction (arrowheads). Scale bars, left 125µm, right 62.5µm. **(d)** Note that the grafted HCC-1 tumouroid tissue recapitulates the histo-architecture of the patient's original tumour (bottom) including the pseudoglandullar rosettes, hallmark of HCC-1 original sample (dashed circle). Scale bars, left 125µm, right 62.5µm. **(e)** Representative H&E (left) and KRT19 (right) immunohistochemistry analyses of CC-1 tumouroids transplanted under the kidney capsule of NSG mice. Scale bar, 125µm. **(f)** Lung metastases derived from CC-1 tumouroids transplanted under the kidney capsule (right panels) were identified using a human specific KRT19 antibody. No metastases were found in the lungs of mice injected with Healthy-1 organoids (left panels). Scale bars, 500µm, magnifications 125µm.

Figure 6. PLC tumouroid lines as a platform for drug screening and validation of actionable therapeutic targets.

(a) Scatterplot of 1-AUC (Area Under the Curve) values from two biological replicates (different passages) of the drug screening data, highlighting drugs (red) having a potential effect on viability (AUC >0.15 for at least 1 of the two replicates) in the indicated tumouroid lines. Each data point is the 1-AUC value for a given drug in a particular tumouroid line. **(b)** Dose-response curves after 6 days treatment with Gemcitabine, Nutlin-3a, LGK974 and SCH772984 generated from the luminescent signal intensities. Data displayed are average of the technical and biological replicates. **(c)** Summary of the different compounds used in the drug screening, the associated pathway and nominal targets and the screen results represented as a summary of the 1-AUC and IC50 data generated for the different tumouroid lines. Red, IC50 within the screen concentration range (detailed in methods); Dense dotted pattern, 1-AUC>0.15 and dose response; scattered dotted pattern, 1-AUC>0.15 and sensitivity at highest concentration only (Supplementary Dataset 5). Compounds highlighted in yellow were selected for further validation. **(d)** Effects on viability of indicated compounds using an organoid formation assay (detailed in methods). Red square, no viable cells; orange square, intermediate sensitivity; no square, resistant. Scale bar, 500µm. **(e)** *In vivo* activity of the ERKi (SCH772984) in CC-1_O tumouroids grafted subcutaneously in NSG mice. Mice were treated with drug/vehicle twice daily for 20 days (n=5 in 2mg/kg of SCH772984 group, n=8 in vehicle group). *, p-value<0.01; **, p-value<0.002 (Mann Whitney test, two-tailed). Results are shown as percentage of the tumour volume relative to day 0 (mean ±SD). **(f-g)** Histological analysis of the antitumor efficacy of SCH772984 on CC-1_O tumours was assessed 24 days after starting the treatment. Representative **(f)** H&E and **(g)** TUNEL staining performed on tissue sections from CC-1_O tumours treated with either vehicle (left) or SCH772984 (right). Representative images from 2 independent experiments are shown. Scale bar, 125µm (H&E) and 25µm (TUNEL).

Supplementary Figure 1: Isolation and culture of primary liver cancer-derived organoids.

We successfully established and expanded human PLC-derived organoids from 7 different PLC patients, including poorly differentiated and moderate/well differentiated HCC (n=2), CC (n=3), and combined HCC/CC (CHC; n=2) by adapting the protocol to isolate and expand liver stem/progenitor cells[24] for: (i) the timing of tissue digestion (2-5 hours to overnight (O/N) according to the degree of liver fibrosis in tumour specimen), (ii) the starting culture conditions (tumouroid specific isolation medium (IM)) and/or (iii) closely monitoring the developing organoid structures (in classical IM, healthy organoids might arise, depending on the type of tumour specimen. In those cases, these are hand-picked upon visual inspection).

After the first passage all tumouroid lines were maintained in the same culture conditions, our previously described "human healthy liver-derived organoid expansion medium"[24-25]. MWP, multi well plate; ROCKi, Rho kinase inhibitor (Y-27632).

Supplementary Figure 2: Patient-derived PLC organoid cultures expand long term *in vitro*.

(a) Tissues (top row) and tumouroids (middle and bottom rows) obtained from HCC-2, HCC-3, CHC-2, CC-2 and CC-3 patients. H&E staining of the tumoural tissues (top), brightfield (middle) and H&E staining (bottom) pictures of tumouroids originated from the corresponding tissues. Scale bars, 125µm (top), 200µm (middle) and bottom 40µm, 125µm, 125µm, 125µm and 70µm (left to right, respectively). **(b-f)** Representative Ki67 nuclear staining performed on patient's tissues included in the study: **(b)** moderately differentiated HCC (HCC-1,-2), poorly differentiated HCC (HCC-3), **(c)** CHC (CHC-1 and CHC-2), **(d)** moderately/well differentiated CC (CC-1,-2) and poorly differentiated CC (CC-3), **(e)** well differentiated HCC (wHCC-8) and **(f)** well differentiated CC (wCC-1). Scale bars, 125µm. **(g)** Ki67-labelling index in PLC tissue samples. The percentage of tumour cells that are positive for nuclear Ki67 labelling was determined by counting a minimum of 1000 cells per patient in at least 2 independent slides. Graph represents mean±SD. Circle, individual data points. **(h)** Brightfield pictures of long-term expanded tumouroid cultures. Scale bar, 200µm. P, passage.

Supplementary Figure 3: Immunohistochemistry and gene expression analyses reveal that PLC tumouroids retain expression patterns of the distinct subtype of the original tumour they derived from.

(a) IHC analysis HepPar1 (hepatocyte/HCC marker) and EpCAM (ductal/CC marker) on CC-3 tissue (_T). Scale bar, 125 µm. **(b)** *EPCAM* expression analysis (q-RT-PCR) in tumour tissues and respective tumouroid lines. Data are normalized to the expression of the housekeeping gene *HPRT*. Graph represents mean±SD of 2 independent experiments. Circle, individual data point. **(c)** PAS-diastase staining on tumoural tissues. Arrowheads mark positive PAS-diastase staining in CHC-1, CC-1 and CC-3 tissues (_T). Scale bar, 62.5 µm. **(d)** *SALL4* expression analysis (q-RT-PCR) in tumour tissues and respective tumouroid lines. Data are normalized to the expression of the housekeeping gene *HPRT*. Graph represents mean±SD of at least 2 independent experiments. Circle, individual data point.

Supplementary Figure 4: Transcriptomic analysis of tumouroids and matching tissues.

(a) PCA analysis of the technical (same sample re-run) (**a**) and biological (same line different passage) (**b**) replicates. Each data point represents one sample. Dot, tumouroid line; triangle, PLC tissues. Of note, since the PCA analysis confirmed that technical and biological replicates are very close we averaged them for each patient line and in the manuscript we show the analysis per averaged patient sample. **(c)** Hierarchical clustering analysis of human primary liver cancer tissue samples based on gene expression (FPKM). Samples analyzed include human primary liver cancer specimens from publically available TCGA cohorts (TCGA-HCC, 344; TCGA-CC, 31) and the tumour specimens included in this study (HCC-1, -3 and CHC-1, -2 and CC-1, -2, -3 tissues). **(d)** Heatmap analysis of the log2 RPKM values (raw z-scored) of selected genes found highly expressed (red) in HCC and/or CHC and/or CC tumour specimen and corresponding tumouroids.

Supplementary Figure 5: Gene expression, immunohistochemistry and functional analyses reveal that the tumouroids retain the differentiation state of their original tissue, even after long-term expansion in culture.

(a) KRT19 IHC in the tissues used in this study. Scale bar, 125 µm. **(b)** IF analysis for the hepatocyte markers ALB and HFN4A (red) and ductal/CC marker KRT19 (green) on tumouroids expanded in culture for at least 3 months. Nuclei were counterstained with Hoechst33342 (blue). Scale bar, 30µm. **(c)** Representative GSEA plots for 2 gene-sets associated with PLC differentiation [HCC with hepatocyte differentiation features (Hoshida et al., 2009) and cholangiocarcinoma[39]] enriched in the tumouroid lines (_O). **(d)** Representative GSEA plots for 1 gene-set describing genes positively correlated with KRT19 expression (Govaere et al., 2013) in the tumoural tissues (_T). +, significantly upregulated; -, significantly downregulated; ns, non significant (FDR>25%). **(e)** Albumin secretion assessed by ELISA in the supernatant from HCC and CHC tumouroids. **(f)** Total bile acid production in HCC tumouroids. **(g)** *KRT7* expression analysis (q-RT-PCR) in tumour tissues and tumouroid lines. Data is normalized to the expression of the housekeeping gene *HPRT*. All graphs (**e-g**) represent mean±SD of 2 independent experiments. Circle, individual data point.

Supplementary Figure 6: Tumouroids recapitulate the genetic alterations present in the original tumour.

(a-b) Whole exome sequencing analysis of patient's tumour tissues and corresponding tumouroid cultures expanded for < 2 months (early passage) or >4 months (late passage) in culture. All variants identified in all samples (21 total; 7 patients with 3 samples (Tissue/early organoid/late organoid)) were used for the global analyses (a) after filtering for quality control as detailed in methods. For (b) a cancer-related set of variants was defined as detailed in methods. **(a)** Percentage of the 6 types of SNVs on transcribed and non-transcribed strand averaged across all samples. Graph represents mean±SD. **(b)** Summary table describing the coding concordant somatic acquired alterations present in all 3 samples per patient (tissue, tumouroids early and late passage). Red, deleterious variants among missense and structural variants (SIFT score <0.05 or N/A). **(c)** Representative GSEA plots for 1 gene-set describing genes up-regulated in tumours developed by transgenic mice overexpressing an EGF secreted form in liver[46] significantly positively enriched in some of the tumouroid lines (_O). +, significantly positively enriched (FDR<25%, p-value<0.05); ns, non-significant (FDR>25%).

Supplementary Figure 7: Transplantation of PLC tumouroids in immunodeficient mice.

(a) CC-2 and CC-3 tumouroids expanded for at least >3 months in culture were transplanted subcutaneously (posterior flanks) on immunocompromised NSG mice and analysed for the presence of tumour growth. Table summarizing the number of cells, site of engraftment and analysis of tumour in the different mice. **(b)** Representative images of the tumour growth after transplantation of tumouroids under the skin (SC) of immunodeficient mice. **(c)** Ki67 staining on xenografts developed under skin (SC) revealed that the tumours were highly proliferative. Scale bar, 125µm (top), 62.5µm (magnification). Similar data was obtained on xenografts developed under kidney capsule (data not shown). **(d)** Representative H&E staining of CC-2 tumouroids transplanted subcutaneously (SC) into NSG mice and corresponding CC-2 patient's tumour tissue (bottom). Scale bars, 125µm (black), 62.5µm (inset). **(e-f)** Tumouroids were re-derived and expanded from xenografts derived from CC-1 tumouroids transplanted into the kidney capsule (Kid.Cap.) or HCC-1 tumouroids transplanted subcutaneously (SC) into immunocompromised NSG mice. **(e)** Representative brightfield and H&E staining images obtained after 5 passages in culture. Scale bar, 500µm (brightfield, top left), 200µm

(brightfield, top right) and 125µm (H&E staining). **(f)** Ploidy analysis of CC-1 and HCC-1 tumouroids rederived from xenografted tumours. Number of metaphases counted, CC-1_O_Kid.Cap.#1, n=15; CC-1_O_Kid.Cap.#2, n=16, HCC-1_O_SC#1, n= 12. Experiment was performed at least in duplicate. Note that morphology, histology and chromosome counts are maintained when comparing the parental tumouroids (derived directly from patient's tumour) and the tumouroids rederived after xenografting. **(g)** Representative brightfield images of tumouroids transplanted under the kidney capsule (Kid.Cap.) of immunodeficient mice. Scale bar, 2 mm. **(h)** Representative brightfield images of lung metastasis found on mice grafted with CC-1 tumouroids under the kidney capsule. Scale bar, 2mm. Magnification 2x.

Supplemental Figure 8: PLC tumouroid lines can be used to identify gene-drug associations that may facilitate personalized therapy.

(a) Scatterplot of area under the dose-response curve (AUC) values obtained for the drugs that were used to validate the drug screening using the tumouroid formation assay presented in Fig. 6d (Gemcitabine, Taselisib, Dasatinib, AZD8931 and SCH772984). Plots show the correlation between the two biological replicates for each tumouroid line. Each data point represents the area under the dose-response curve (1-AUC) value. Red, sensitive. Triangle, result further validated in the tumouroid formation assay. **(b)** Western blot analysis for phosphorylated ERK1/2 (P-ERK) and total ERK (ERK) in HCC1 and CC-1 tumouroid lines treated for 24 hours with either the pan-ERBB inhibitor AZD8931, the ERK inhibitor SCH772984 or with the vehicle. AZD8931 reduced ERK phosphorylation in HCC-1_O line only, whereas SCH772984 potently inhibited ERK phosphorylation in both HCC-1_O and CC-1_O lines, as expected according to their mutational profile (HCC-1_O, *KRAS* WT and CC-1_O, *KRASG12D*; see Fig. 4). Total ERK was used as loading control. Representative blots of 2 independent experiments are shown. **(c)** *In vivo* activity of SCH772984 in HCC-1_O tumouroids grafted under the skin of NSG mice. Mice were treated with drug/vehicle twice daily for 15 days (n=3 in 2mg/kg of SCH772984 group, n=2 in vehicle group). Significant differences between the SCH772984 and the vehicle treated groups were observed. *, p-value<0.01 and **, p-value<0.002 (t-test, two-tailed). Results are shown as percentage of the tumour volume relative to day 0 (mean ±SD). **(d)** Histological analysis of the antitumour efficacy of SCH772984 on HCC-1_O tumours. Representative H&E staining on tissue sections from HCC-1_O tumours treated with either vehicle (left) or SCH772984 (right). Representative images of 2 independent experiments are shown. Scale bar, 125uM. **(e)** Western blot analysis for phosphorylated ERK1/2 (P-ERK) and total ERK (ERK) in CC-1 xenografted tumours dissected 6 hours after injecting SCH772984 (2mg/kg) or vehicle intratumourally. Total ERK was used as loading control. Representative blots of 2 independent experiments are shown.

Supplementary Table 1: Patients' information and organoid efficiency derivation and expansion.

Table summarizing the patient's and healthy donor information including gender, age, type of tissue, histological analysis, Ki67 index and serum AFP levels. Organoid growth and expansion are indicated when appropriate. Efficiency of derivation and efficiency of organoid expansion are calculated. Note that all healthy tissues derived from healthy donors undergoing liver transplantation. N/A, not applicable; N/T, not tested.

*Organoids from HCC-NL1 patient (derived at Erasmus Rotterdam Centre) became infected after some weeks in culture, and therefore were excluded from the analysis.

Supplementary Dataset 1: RNAseq data analysis.
Dataset including S1-S8 tables summarizing all the RNAseq data analyses except GSEA (see Supplementary Dataset 2 and 3) and the TCGA analyses (survival & clustering). Used for Fig. 3 and Supplementary Fig. 4.

Supplementary Dataset 2: Tumouroids GSEA data.
Dataset including S1-S15 tables summarizing the tumouroids GSEA data used for Fig. 3 and Supplementary Fig. 5, 6 and 8.

Supplementary Dataset 3: Tissue GSEA data.
Dataset including S1-S15 tables summarizing the tissues GSEA data used for Fig. 3 and Supplementary Fig. 5, 6 and 8.

Supplementary Dataset 4: WES.
Dataset including S1-S15 tables summarizing the coding cancer-related variants found in short (early) and long (late) term expanded cultures and corresponding tissues used for Fig. 4g and Supplementary Fig. 6b.

Supplementary Dataset 5: Drug screening.
Dataset including S1-S2 tables summarizing the List of drugs screened, their concentration and the data used for Fig. 6 and Supplementary Fig. 8

Supplementary Dataset 6: List of antibodies, kits, and primers used.

ONLINE METHODS

General experimental approaches.

No samples, mice or data points were excluded from the reported analyses. Detailed information on experimental design and reagents is available through the accompanying Life Sciences Reporting Summary and Supplementary Dataset 6. Raw data used to generate figures are provided in Datasets 1-6 and Source data files 1 and 2.

Human specimens

Liver tumour specimen (~1-4 cm3) were obtained from resection performed at Erasmus Medical Center Rotterdam (MEC-2013-143), Cambridge University Hospitals NHS Trust (REC: 15/LO/0753 - Approval by NRES Committee London – Westminster) and The Royal Infirmary Hospital Edinburgh (REC: 15/ES/0097) on patients who had no history of viral-meditated hepatitis (excluded under Institutional safety guidelines). Handling and processing of samples was performed according to HTA guidelines. Healthy liver resections (~1cm3) were obtained during liver transplantation performed at the Erasmus Medical Center, Rotterdam MEC-2014-060 and at the Cambridge University Hospitals NHS Trust REC: 15/EE/0152. The Cambridge samples were provided by the Cambridge Biorepository for Translational Medicine (CBTM). All patients provided informed consent. Samples were procured and the study was conducted under Institutional Review Board approval prior to tissue acquisition. Samples were confirmed to be tumour or normal based on histopathological assessment. The diagnosis of each case was confirmed on routine hematoxylin and eosin-stained slides by an independent histopathologist. For each tumour specimen, samples were split into 4 parts and processed for histology, RNA and DNA isolation, or dissociated and processed for organoid culture.

Isolation and Culture of human liver healthy and tumoural organoids

Healthy liver-derived organoids were isolated and cultured using our previously described method[24,25] while tumour-derived organoids (tumouroids) were isolated by adapting this method as follows. Briefly, ¼ of the patient-derived or healthy donor specimen (~0.25 to 1cm3) was minced and incubated at 37°C with the digestion solution. Incubation was performed for 30min-1h for healthy donor tissue (as described in ref 24) while for patient-derived tissue digestion was left for 2-5 hours to overnight (O/N) according to the degree of liver fibrosis, which was evaluated in a patient-specific basis by visual inspection under a stereomicroscope as well as according to the resistance of the tissue to be minced. For patient-derived tissue, after 2-5h digestion, the digestion preparation was visually inspected and either digestion was stopped or, if a significant part of the original tissue was still under-digested (>50% of starting material, depending on the fibrotic status of the tissue), the preparation was left o/n at 37°C in the digestion solution, in order to get a good yield of tumoural cells. This increase in the digestion times compared to healthy tissue (>2h-o/n) facilitated reducing the number of viable healthy contaminating duct cells. In all cases, the digestion was stopped once no pieces of tissue were left, and the suspension was then filtered through a 100µm nylon cell strainer and spun 5 min at 300-400G. The pellet was washed in cold Advanced DMEM/F12 (GIBCO) then mixed with BME (Basement Membrane Extract, Type 2, Pathclear). 2.000-5.000 cells were seeded per well in a 24-multi-well plate. After BME had solidified, half of the wells obtained for each sample were cultured in the classical human liver organoid isolation medium (Advanced DMEM/F12 supplemented with 1% Penicillin/Streptomycin, 1% Glutamax, 10 mM HEPES, 1:50 B27 supplement (without Vitamin A), 1:100 N2 supplement, 1.25mM n-Acetyl-L-cysteine, 10% (vol/vol) Rspo-1 conditioned medium, 30% (vol/vol) Wnt3a conditioned medium, 10mM nicotinamide, 10nM

recombinant human [Leu15]-Gastrin I, 50ng/ml recombinant human EGF, 100ng/ml recombinant human FGF10, 25ng/ml recombinant human HGF, 10µM Forskolin, 5µM A8301, 25ng/ml Noggin and 10µM Y27632 as described in ref 24). The other half were cultured in a tumouroid specific isolation medium (classical human liver organoid isolation medium without Noggin, Rspo-1 and Wnt3a conditioned media but supplemented with 3nM Dexamethasone (Sigma Aldrich). Thus, the tumoroid isolation medium contained: Advanced DMEM/F12 supplemented with 1% Penicillin/Streptomycin, 1% Glutamax, 10 mM HEPES, 1:50 B27 supplement (without Vitamin A), 1:100 N2 supplement, 1.25mM n-Acetyl-L-cysteine, 10mM nicotinamide, 10nM recombinant human [Leu15]-Gastrin I, 50ng/ml recombinant human EGF, 100ng/ml recombinant human FGF10, 25ng/ml recombinant human HGF, 10µM Forskolin, 5µM A8301, 10µM Y27632 and 3nM Dexamethasone). It is important to always culture half of the sample in classical isolation medium and half in our tumouroid specific isolation medium, to ensure growth of the cultures. For instance, CC-1 patient material only grew in classical isolation medium because it requires Rspo-1 to grow. For this line, though, we enriched for the tumouroids by hand-picking out contaminating healthy organoids (as described in Supplementary Fig. 1).

After isolation medium was changed twice a week. For healthy-donor derived organoids, isolation medium was changed to "human healthy liver-derived organoids expansion medium" after 1-week in culture (see composition below). For tumouroids, isolation medium (classical or tumouroid specific) was maintained until the first split. For tumouroid culture establishment, after 2-3 weeks in culture (depending on the sample) the growing structures were visually inspected and, if required, contaminating healthy organoids were hand-picked to prevent these from outgrowing the tumouroid structures. Upon attainment of dense culture (healthy liver-derived organoids (1-2 weeks after isolation) and tumour-derived organoids (2-3 weeks after isolation) were passaged by mechanical dissociation into small fragments via trituration with a glass Pasteur pipet, and transferred to fresh matrix in the previously defined "human healthy liver-derived organoids expansion medium"[24,25] : Advanced DMEM/F12 supplemented with 1% Penicillin/Streptomycin, 1% Glutamax, 10 mM HEPES, 1:50 B27 supplement (without Vitamin A), 1:100 N2 supplement, 1.25mM n-Acetyl-L-cysteine, 10% (vol/vol) Rspo-1 conditioned medium, 10mM nicotinamide, 10nM recombinant human [Leu15]-Gastrin I, 50ng/ml recombinant human EGF, 100ng/ml recombinant human FGF10, 25ng/ml recombinant human HGF, 10µM Forskolin and 5µM A83-01)[24]. Expansion medium was changed twice a week and cultures were split upon attainment of dense culture.

All cultures were tested every month for mycoplasma using the 'PCR Mycoplasma Test kit I/C' kit from Promega in accordance with the manufacturer's instructions.

To prepare frozen stocks, organoid cultures were dissociated and mixed with recovery cell culture freezing medium (GIBCO) and frozen following standard procedures. When required, the cultures were thawed using standard thawing procedures and cultured as described above. For the 3-4 days (organoids) or first 2 weeks (tumouroids) after thawing, the culture medium was supplemented with Y-27632 (10µM). Organoid pictures were taken with either a Leica M80 stereoscope and Leica MC170 HD camera or with an inverted microscope Leica DMIL and Leica DFC 450C camera.

Histology and staining

Tissues and organoids were fixed for 24 or 0.5 hours respectively, in 10% neutral buffered formalin (Sigma), at room temperature, and then embedded in paraffin as follows: briefly, tissues were processed through a graded ethanol series followed by xylene, and then

embedded in paraffin, cut at 5µm and stained (H&E and immunohistological staining). For immunofluorescence experiments fixed organoids were rehydrated with PBS following formalin fixation. For immunohistological staining, paraffin slides were deparaffinised and subjected to antigen retrieval using citrate sodium solution pH=6. To reduce background nonspecific staining, and permeabilise the sample, slides were incubated with a 3% BSA, 0.5% Triton in TBS solution for 1 hour. Primary antibodies (listed in the Supplementary Dataset 6) were then applied at appropriate dilutions for overnight at 4°C (see Supplementary Dataset 6 for details). Endogenous peroxidase activity was blocked for 15 min in a 3% hydrogen peroxide/methanol buffer. Detection of bound antibody was accomplished with the BrightVision Ultimate kit (Immunologic). Briefly, slides were washed in TBS and incubated with a secondary antibody-HRP conjugate for 1 hour at room temperature and finally developed with 3,3′-diaminobenzidine (DAB) for 5 min, counterstained with haematoxylin, and mounted with DPX (Sigma). Slides were also stained in the absence of primary antibodies to evaluate nonspecific secondary antibody reactions. For TUNEL assay, Click-iT Plus TUNEL kit (Molecular Probes, Life technologies) was used in accordance with the manufacturer's instructions. Pictures were taken with a Leica microscope DM 4000 microscope and DFC 450 camera (Leica). For whole mount immunofluorescence staining, organoids were processed as described in [23,24] [25]. Briefly, organoids were incubated over 2 to 3 nights at 4°C, washed in PBS, and revealed by incubation with a secondary antibody conjugated to a fluorophore. Nuclei were stained with Hoechst33342 (Molecular Probes, Life technologies). Confocal images were captured on a Leica SP5 inverted confocal microscope (Leica).

Ki67 index

Each tumour slide stained for Ki67 was manually scanned with a microscope at ×10 objective, and the area of greatest Ki67 positivity (hot spot) was selected for photographing. At least 1000 total tumoural cells were counted on a total of 2 independently stained slides per patient. Pictures were taken with a Leica microscope DM 4000 microscope and DFC 450 camera (Leica) and Ki67-negative and -positive were then counted using ImageJ "cell counter" plugin. Light brown or pale staining nuclei were ignored during counting.

Karyotyping

Karyotyping was performed as previously described [24]. Briefly, cultures were incubated with 0.1ug/ml Karyomax Colcemid (Gibco). After 24 hours, organoids were harvested and dissociated using TrypLE (Gibco). Cells were incubated with KCL 0.0075M hypotonic solution for 10 min, fixed in methanol:acetic acid (3:1) and dropped on a microscope slide for visualization. Nuclei were mounted and stained using Vectashield with DAPI (Vector Labs). A minimum of 15 metaphases per sample were counted.

Sequencing and analysis

For both RNA-Sequencing (RNASeq) and Whole-Exome Sequencing (WES), low quality reads were filtered (<Q20) followed by trimming of low quality bases from the ends of the reads (<Q20). Adaptors were also removed using cutadapt.

RNA-Sequencing. RNA was isolated from organoids using RNeasy mini kit (Qiagen) following manufacturer's instructions. RNA libraries were prepared for sequencing using the Smartseq2 method. RNA sequencing was performed using Illumina HiSeq sequencer (50bp single-end reads and 10-20 million reads were generated for each sample). Reads were aligned with Tophat (v2.1.0)[57] to the GRCh38.82 genome, using the corresponding gtf file for exon positions. Counts were generated using featureCounts (v1.5.0-p1)[58]. Only protein-coding genes, lincRNAs, processed transcripts and misc RNA were kept for further study. Normalised counts were created using DESeq2[59] and RPKMs using edgeR's function [edgeR]. The technical and biological replicates (different passages) were merged. Healthy growing in expansion and differentiation medium and corresponding tissues were used as additional controls.

To assess concordance of tissues with organoids genes were filtered and the Pearson's correlation coefficient was calculated pairwise between tissues and organoids. The correlation matrix was then z-scored. The principal components for several subgroups of the samples were calculated from the normalised DESeq counts, and the first two (PC1, PC2) were plotted. We then analysed the top 100 genes with highest loadings across PC2, which separated the samples by subtype. Functional analysis was split across the three subtypes, and genes were excluded in each unless healthy or tumour samples had RPKM values greater than 1. To generate a statistic for tumoural tissue samples, the log2 fold change (FC) of each tumoural tissue was divided by the mean of the healthy tissues. To generate a statistic for HCC tumouroid samples, two log2 fold changes (FC) were calculated: the first was HCC organoid divided by the mean of healthy liver-derived organoid and the second was HCC tissue divided by the mean of the healthy tissues. Then the mean or minimum was then taken of these two ratios, whichever had a lower absolute value. The same statistic was generated for CHC and CC tumouroids using the mean healthy tissue instead of healthy liver-derived organoid as a baseline for the first fold change. These statistics were then used for pre-ranked gene set enrichment analysis using GSEA software (http://www.broadinstitute.org/gsea/)[60]. 159 gene sets were used for running the GSEA. These gene sets were obtained after curation of the publically available C2 MSigDB collection for "LIV", "HEPT" and "STEM" key words and completed by available liver cancer gene set described in literature (see Supplementary Dataset 2 and 3) in order to select a relevant list of gene sets associated with liver cancer and stemness. 1,000 permutations were used to calculate p-value. A tumouroid signature was identified by finding genes with the highest FC when dividing the minimum expression value, in RPKMs, over all tumouroid samples by the mean of the expression of healthy liver-derived organoids in differentiation medium. Several aspects of the genes defining the tumouroids' signatures were annotated: the description of their corresponding proteins was downloaded from Uniprot[61], and their relevance to disease by retrieving the Disease Ontology terms (using the R package dnet v1.0.10[62]).

WES. DNA from tumour tissue and matched tumouroid lines was extracted using DNeasy Blood & Tissue Kit (Qiagen) according to manufacturers' protocol. Point mutations and short indels were called in a procedure composed of several steps as follows: **(i)** Reads were aligned to the UCSC hg38 genome using Bowtie2 (v2.2.6)[63] and the output was preprocessed for variant calling by marking duplicates with Picard (v1.113) (http://broadinstitute.github.io/picard/) followed by Indel realignment with the GATK toolkit (v3.7)[64]. SNPs and Indels were called with Varscan (v.2.3)[65]. **(ii)** We identified and selected the variants with the following parameters: base quality ≥15 (Phred score), read depth ≥15 and annotated by SNPEff[66] as not "intergenic". **(iii)** We removed variants on alternate

haplotypes. **(iv)** Analysis was then split between patients. For each, there were 3 samples, the tissue and the corresponding tumouroids expanded for <2months (early) or >4months (late). If a variant was called in the 'early' sample, a variant was added in the tissue if its pileup showed evidence of the same variant at that position. Moreover if a variant was called in the 'late' sample, a variant was added in the tissue and early sample if their pileup both showed evidence of the same variant at that position. Fig. 4c-e and Supplementary Fig. 5a are based on this final list of variants. To assess concordance, overlaps of variants found in tissue and early and late tumouroids were calculated within and between cancer types using GATK (v3.7). The mutation spectrum was examined in each sample in both non-transcribed and transcribed strands and then summarized by representing the average proportion across all samples. A cancer-related set of variants was defined by adding the following filtering steps: **(v)** To filter out polymorphisms and non-damaging variants we exclude variants which had reads supporting variations ≥ 2 in our sequenced healthy samples (Healthy-1_Tissue and _Organoid; Healthy-2_Organoid) and / or were included in dbSNP (common _ no _ known _ medical _ impact _ 20170801.vcf)[67] and / or with a frequency >0.01 in ExAC database[68]. To select for cancer related variants we then **(vi)** filter for the variants present in COSMIC (v76)[69], and **(vii)** synonymous and intronic variants were filtered out. The variant positions with their associated effects were annotated with SnpEff[66]. Resultant variants were used for the Fig. 4f. **(viii)** Finally, we selected the mutations that were highly predicted to impair the function of the corresponding encoded proteins by filtering for coding mutations and using SIFT[70]) to predict the deleterious (SIFT score <0.05) impact of missense and structural variants. A summary of the concordant (tissue/early/late) coding variants obtained per patient is provided in Supplementary Dataset 4 and this final list of variants was used for Supplementary Fig. 6b and Fig. 5g.

Accession Numbers

All RNA-seq and WES data are available at Gene Expression Omnibus (GEO) under accession number GSE84073.
https://www.ncbi.nlm.nih.gov/geo/query/acc.cgi?acc=GSE84073

The Cancer Genome Atlas (TCGA) analyses

We used public available data generated by the TCGA Research Network: http://cancergenome.nih.gov/ to perform hierachical clustering and survival outcome analyses. FPKMs were downloaded from the Genomic Data Commons Data Portal (GDC), using GDC's API, for the projects TCGA-LIHC (374 tumoral samples (ICD-O-3 number=C22.0) and 50 normal control samples) and TCGA-CHOL (31 tumoral samples (ICD-O-3 number=C22.1) and 8 normal control samples).
For the hierarchical clustering our sequencing data was processed according to the GDC mRNA quantification analysis pipeline to obtain FPKM values comparable with the ones from the TCGA-cohorts. The hierarchical clustering used the Euclidean distances between samples based on the top 500 expressed genes and was performed using hclust in R and plotted using the dendextend R package[71]. Healthy, not annotated for the stage of the disease and recurrent disease samples were excluded from the analysis.
For the survival analysis we examined the expression of the top 30 genes of the tumouroid signature, in both TCGA-LIHC and TCGA-CHOL cohorts. From the FPKM values of tumoral and control samples we generated base R boxplots (R's default boxplot code) and

assess the significance between both group by unpaired two-tailed t-test. Survival plots were created using the R package TCGAbiolinks (v2.2.10)[72] and by splitting, per gene, the tumour samples into high- and low-expression groups. The median of all samples was used as the threshold and significance for differences between the two groups was assessed by log-rank test.

Quantitative RT-PCR

Total RNA was extracted from organoid cultures or freshly isolated tissues using RNeasy mini kit (Qiagen) in accordance with the manufacturer's instructions. cDNA was synthesized using 0.5µg of total RNA and a M-MLV Reverse Transcriptase kit (Promega). cDNA was amplified with iTaq™ Universal SYBR Green Supermix (BioRad) and using gene-specific primers described in Supplementary Dataset 6). All targets were amplified (40 cycles) on a CFX96 Touch Real-Time PCR Detection System (Biorad). Data were analyzed using BioRad CFX manager. Expression levels were normalized to the expression of the housekeeping gene *HPRT*.

Functional *in vitro* studies

Functional studies were performed in collected supernatant or in whole organoids. To assess albumin production, culture medium was collected 1 week after the last medium change and albumin levels were assessed using an Albumin ELISA kit (Assay Pro) according to manufacturer's instructions. Values were corrected for time and cell number. Concentration of total bile acid was established using a Total Bile Assay kit (Cell Biolabs, inc.) according to manufacturer's instructions on supernatant obtained after sonication of whole organoids in PBS.

Organoid formation Assay

To assess the organoid formation efficiency in classical *vs* tumouroid isolation medium, pictures of all full drops of BME obtained per patient were photographed using a Leica M80 stereoscope 2-3 weeks after isolation (depending on the sample) and all viable tumouroid structures were counted.
For the drug sensitivity assays, organoids were dissociated into 2-5 cell clumps by enzymatic dissociation with TrypLE (Life Technologies). Then, cell viability assays were conducted by plating 500 clumps per well of a 48-well cell culture plate in 250µl of expansion medium supplemented with 0.5 µM Gemcitabine (Actavis), or 5 µM of AZD8931 (Selleckchem), or 10µM of SCH772984 (Selleckchem) or 2µM Dasatinib (Selleckchem) or 10µM of Taselisib (Selleckchem) or 3µM of IWP2 (Sigma Aldrich) or 1µM of Gefitinib (Selleckchem) or vehicle (DMSO) control. All conditions were supplemented with Rho kinase inhibitor Y-27632 (Sigma-Aldrich). The concentration selected for each compound was based on the cell viability data from our laboratory, the results from the screening or the literature. Medium was changed 3 times a week for 3 weeks. Viable cells were assessed by their ability to generate organoid *de novo*. Representative pictures of the viability result were taken 2-3 weeks after starting the treatment. All cell viability experiments were conducted in triplicate in at least two independent experiments (biological replicates = different passages).

Drug screening

Organoid viability assays were conducted as previously described[19,50]. Briefly, 8µl of ~7mg/ml BME-2 was dispensed in to 384-well microplates and allowed to polymerize. Organoids were mechanically dissociated by pipetting before being resuspended in 2% matrigel/growth media (15.000-20.000 organoids/ml) and dispensed into 384-well plates. The following day a concentration dilution series of each compound was dispensed using liquid handling robotics and cell viability assayed using CellTiter-Glo® (Promega) following 6 days of drug incubation. An experimental concentration range was calculated for each compound using a 7-point half-log dilution series of the highest maximal concentration. The maximal concentration of each compound can be found in Supplementary Dataset 5. Screens were performed in technical (same screening run) and biological duplicates (different passage), and all screening plates were subjected to stringent quality control measures and a Z-factor score comparing negative and positive control wells was calculated. Dose–response curves were fitted to the luminescent signal intensities utilizing a method previously described[73]. Variation in replicates was greater than similar screens performed in colorectal tumouroids and was likely due to the large size of HCC tumouroids leading to uneven distribution in screening wells[19,50]. Compound and screening concentrations are provided in Supplementary Dataset 5. The range of concentrations selected for each compound was based on *in vitro* data of concentrations inhibiting relevant target activity and cell viability based on data from our laboratory or literature.

Mouse xenograft studies

All mouse experiments have been regulated under the Animals (Scientific Procedures) Act 1986 Amendment Regulations 2012 following ethical review by the University of Cambridge Animal Welfare and Ethical Review Body (AWERB) and have been performed in accordance to the Home Office license awarded to M.H. For subcutaneous grafts, 1 million cells suspensions were prepared in PBS-0.1%BSA (CC and healthy liver-derived organoid lines) or in Advanced DMEM/F12 (GIBCO) 1% glycosil (ESI-BIO) further supplemented with 50 ng/ml each of HGF and VEGF (HCC and healthy liver-derived organoid lines) and were injected into both flanks of male NSG-NOD scid gamma mice (Charles River). Visible tumours developed in approximately 2–4 weeks (CC organoid lines) and 4-6 months (HCC-1 organoid line). Mice were culled when the tumour reached limit end-point (size or ulceration). For kidney capsule graft, cell line suspensions were prepared in Advanced DMEM/F12 (GIBCO) with BME2 (7mg/ml) and 500.000 cells were implanted under the renal capsule of NSG mice. These mice were then culled at different time point (0.5, 1, 2 and 3 month) and kidney and lung tissues were harvested to assess the growth and the metastatic potential of the grafted cells.

To assess the efficiency of the ERK inhibitor SCH772984 *in vivo* mice with established subcutaneous tumours were randomized to drug treatment by splitting size-matched tumours in two groups (SCH772984/vehicle). Treatments (SCH772984 at 2 mg/kg, or an equal volume of vehicle (25%DMSO-30%PEG300 in DD water) were administered by intratumoural injection twice daily for 15 (CC-1 tumouroid line) or 20 (HCC-1 tumouroid line) days. Tumour sizes were measured 3 times a week after the first week of treatment using a caliper and volumes were calculated by applying the formula $v = 0.5 \times L \times w \times h$, where v is volume, L is length, w is width and h is height. Investigators performing tumour measurements were blinded to treatment groups. Histological analyses of the tumours from both CC-1 and HCC-1 lines were performed at 24 and 25 days after treatment initiation respectively.

Western blot assay

Cell lysate for Western blotting were prepared from **(i)** ice-cold PBS washed tumouroids (to remove the basement matrix) grown for 24 hours in expansion medium supplemented with 10μM of SCH772984 (Selleckchem), or 5 μM of AZD8931 (Selleckchem) or equal volume of vehicle (DMSO) and from **(ii)** CC-1 xenografted tumours, 6 hours after intratumoural injection of 2mg/kg of SCH772984 (Selleckchem) or equal volume of vehicle. Lysates were made in ice-cold buffer consisting of 50mM Tris-HCl (pH 7.4), 150mM NaCl, 2mM EDTA, 50mM NaF, 1% triton, 1% NP-40. 0.1% SDS, 0.5% Na-deoxycholate, supplemented with 1mM sodium orthovanadate and protease inhibitor cocktail (Roche) (15min on ice for the cells and 30min on ice for the tissues). Protein lysates were cleared by microcentrifugation at 10.000 rpm for 10 min at 4°C and the supernatants aliquoted and stored at −20°C. Equivalent amounts of protein from each sample were separated on 10% SDS-PAGE gels and then transferred by electroblotting onto nitrocellulose membranes. Membranes were then blocked in in PBS-0.1% Tween-5% BSA and immunoblotted with the following antibodies overnight at 4°C: ERK (1/2000), P-ERK (1/3000) (Cell signalling). After washing 3 times in PBS-0.1% Tween, the membranes were incubated for 1h at room temperature with anti-rabbit horseradish peroxidase (HRP)-conjugated secondary antibodies (1:10.000; abcam). Antibody-protein complexes were visualised using ECL Prime Western Blotting Detection Reagent (GE Healthcare).

Statistical Analyses

All summary data are presented as mean ± SD or representative images of at least 2 independent experiments. All statistical analyses were performed in R and GraphPad Prism software (GraphPad 7.0). Sample size (n) values used for statistical analyses are provided in the relevant figures and supplementary figures. Individual data point are graphed or can be found in Source data files. Tests for differences between two groups were performed using Mann-Whitney's two-tailed test, Student's two-tailed unpaired t-test or log-rank test as specified in the figure legends. When using t-test we assumed normality and equal distribution of variance between the different groups. No data points were excluded from the statistical analyses. Significance was set at FDR ≤ 0.25 (for GSEA) and p-value ≤ 0.05 (for all other experiments).

References Methods

57. Trapnell, C., Pachter, L. & Salzberg, S.L. TopHat: discovering splice junctions with RNA-Seq. *Bioinformatics* **25**, 1105-1111 (2009).
58. Liao, Y., Smyth, G.K. & Shi, W. featureCounts: an efficient general purpose program for assigning sequence reads to genomic features. *Bioinformatics* **30**, 923-930 (2014).
59. Love, M.I., Huber, W. & Anders, S. Moderated estimation of fold change and dispersion for RNA-seq data with DESeq2. *Genome Biol* **15**, 550 (2014).
60. Subramanian, A., *et al.* Gene set enrichment analysis: a knowledge-based approach for interpreting genome-wide expression profiles. *Proc Natl Acad Sci U S A* **102**, 15545-15550 (2005).
61. The UniProt, C. UniProt: the universal protein knowledgebase. *Nucleic Acids Res* **45**, D158-D169 (2017).

62. Fang, H. & Gough, J. The 'dnet' approach promotes emerging research on cancer patient survival. *Genome Med* **6**, 64 (2014).
63. Langmead, B. & Salzberg, S.L. Fast gapped-read alignment with Bowtie 2. *Nat Methods* **9**, 357-359 (2012).
64. McKenna, A., *et al.* The Genome Analysis Toolkit: a MapReduce framework for analyzing next-generation DNA sequencing data. *Genome Res* **20**, 1297-1303 (2010).
65. Koboldt, D.C., *et al.* VarScan: variant detection in massively parallel sequencing of individual and pooled samples. *Bioinformatics* **25**, 2283-2285 (2009).
66. Cingolani, P., *et al.* A program for annotating and predicting the effects of single nucleotide polymorphisms, SnpEff: SNPs in the genome of Drosophila melanogaster strain w1118; iso-2; iso-3. *Fly (Austin)* **6**, 80-92 (2012).
67. Sherry, S.T., *et al.* dbSNP: the NCBI database of genetic variation. *Nucleic Acids Res* **29**, 308-311 (2001).
68. Lek, M., *et al.* Analysis of protein-coding genetic variation in 60,706 humans. *Nature* **536**, 285-291 (2016).
69. Forbes, S.A., *et al.* COSMIC: exploring the world's knowledge of somatic mutations in human cancer. *Nucleic Acids Res* **43**, D805-811 (2015).
70. Sim, N.L., *et al.* SIFT web server: predicting effects of amino acid substitutions on proteins. *Nucleic Acids Res* **40**, W452-457 (2012).
71. Galili T. dendextend: An R package for visualizing, adjusting and comparing trees of hierarchical clustering. *Bioinformatics* **31,** 3718–20 (2015).
72. Colaprico, A., *et al.* TCGAbiolinks: an R/Bioconductor package for integrative analysis of TCGA data. *Nucleic Acids Res* **44**, e71 (2016).
73. Vis, D.J., *et al.* Multilevel models improve precision and speed of IC50 estimates. *Pharmacogenomics* **17**, 691-700 (2016).

Figure 1

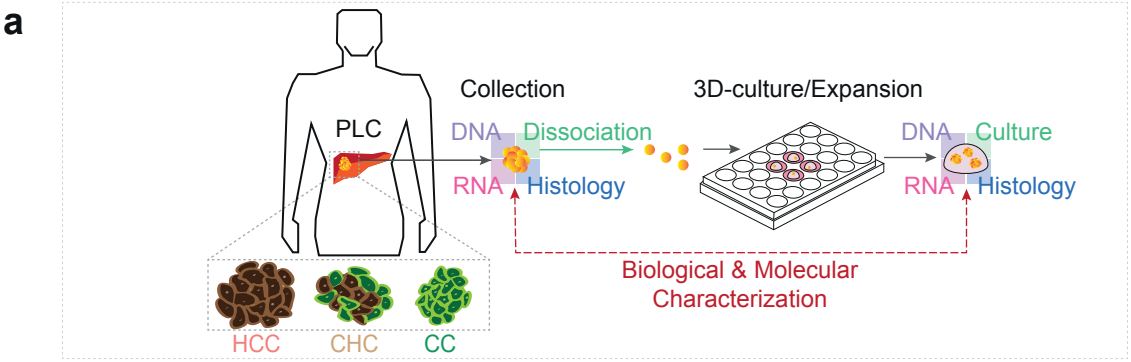
a
PLC
Collection
3D-culture/Expansion
DNA
Dissociation
RNA
Histology
DNA
Culture
RNA
Histology
Biological & Molecular
Characterization
HCC
CHC
CC

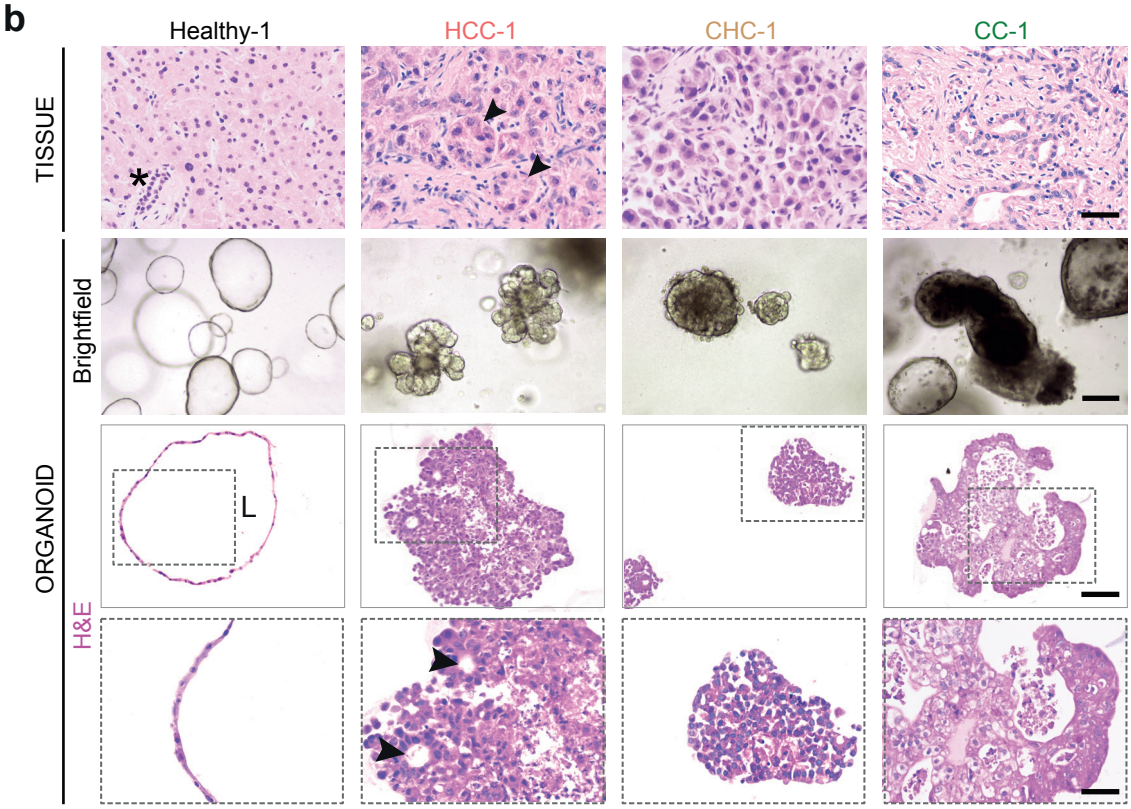
b
Healthy-1
HCC-1
CHC-1
CC-1
TISSUE
ORGANOID
Brightfield
H&E
L

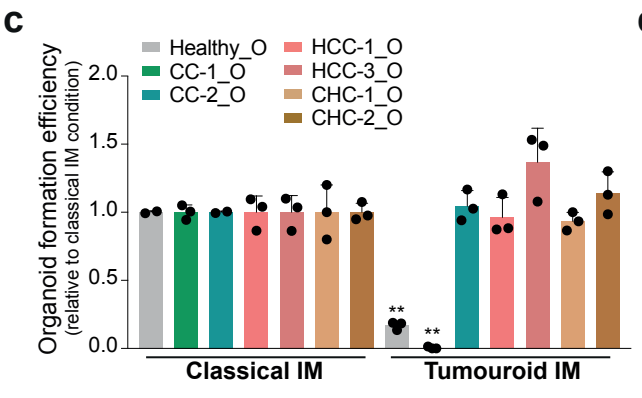
c
Healthy_O
CC-1_O
CC-2_O
HCC-1_O
HCC-3_O
CHC-1_O
CHC-2_O
Organoid formation efficiency
(relative to classical IM condition)
2.0
1.5
1.0
0.5
0.0
**
**
Classical IM
Tumouroid IM

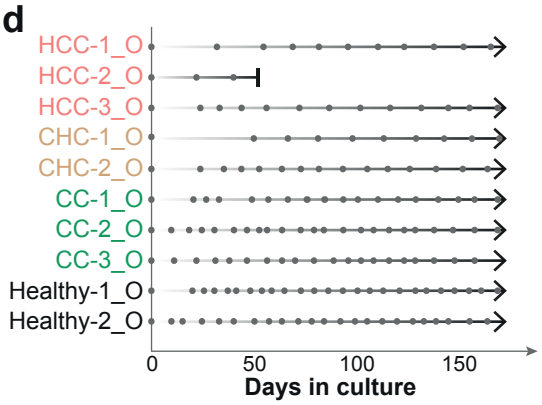
d
HCC-1_O
HCC-2_O
HCC-3_O
CHC-1_O
CHC-2_O
CC-1_O
CC-2_O
CC-3_O
Healthy-1_O
Healthy-2_O
0
50
100
150
Days in culture

Figure 2

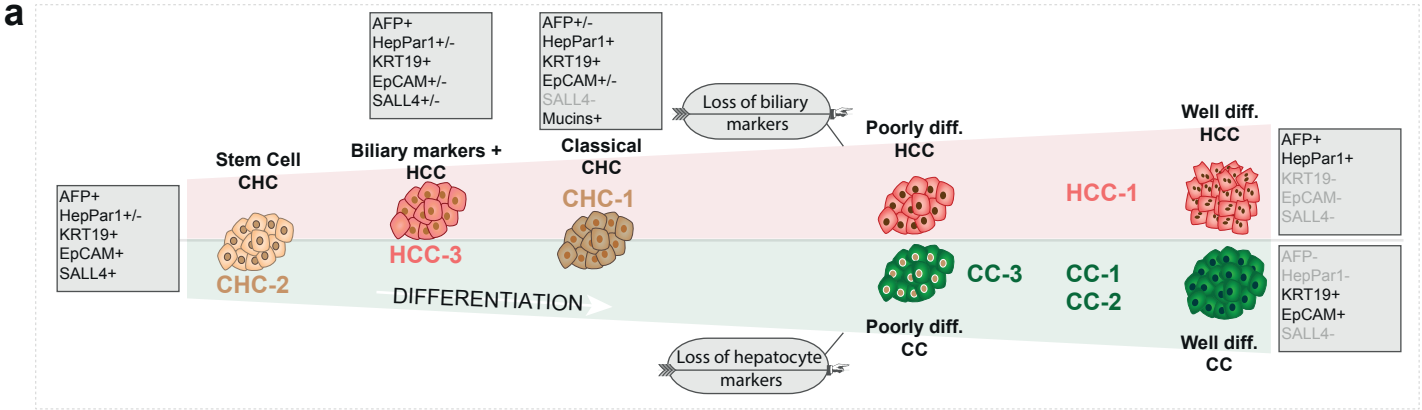
a
AFP+
HepPar1+/-
KRT19+
EpCAM+
SALL4+
Stem Cell
CHC
CHC-2
AFP+
HepPar1+/-
KRT19+
EpCAM+/-
SALL4+/-
Biliary markers +
HCC
HCC-3
AFP+/-
HepPar1+
KRT19+
EpCAM+/-
SALL4-
Mucins+
Classical
CHC
CHC-1
DIFFERENTIATION
Loss of biliary
markers
Poorly diff.
HCC
HCC-1
Well diff.
HCC
AFP+
HepPar1+
KRT19-
EpCAM-
SALL4-
CC-3
CC-1
CC-2
AFP-
HepPar1-
KRT19+
EpCAM+
SALL4-
Loss of hepatocyte
markers
Poorly diff.
CC
Well diff.
CC

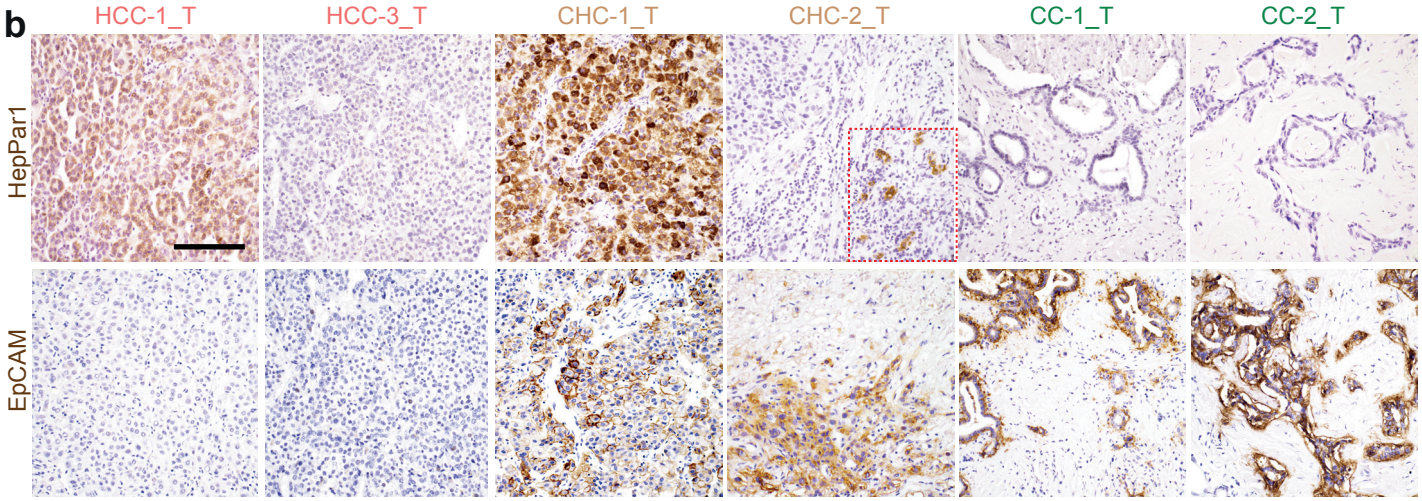
b
HCC-1_T
HCC-3_T
CHC-1_T
CHC-2_T
CC-1_T
CC-2_T
HepPar1
EpCAM

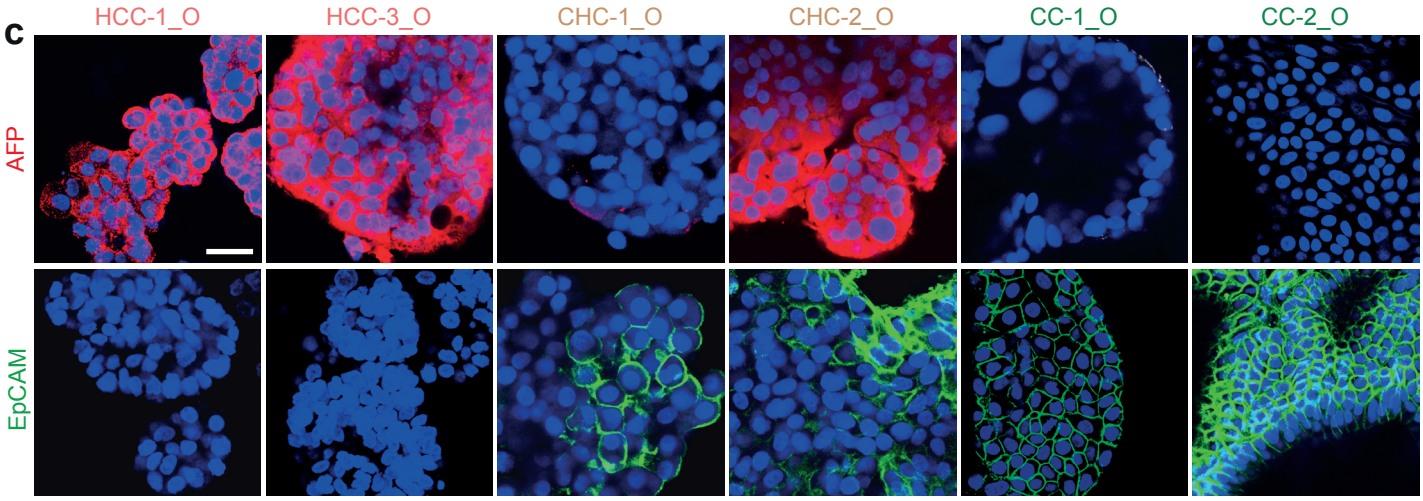
c
HCC-1_O
HCC-3_O
CHC-1_O
CHC-2_O
CC-1_O
CC-2_O
AFP
EpCAM

Figure 3

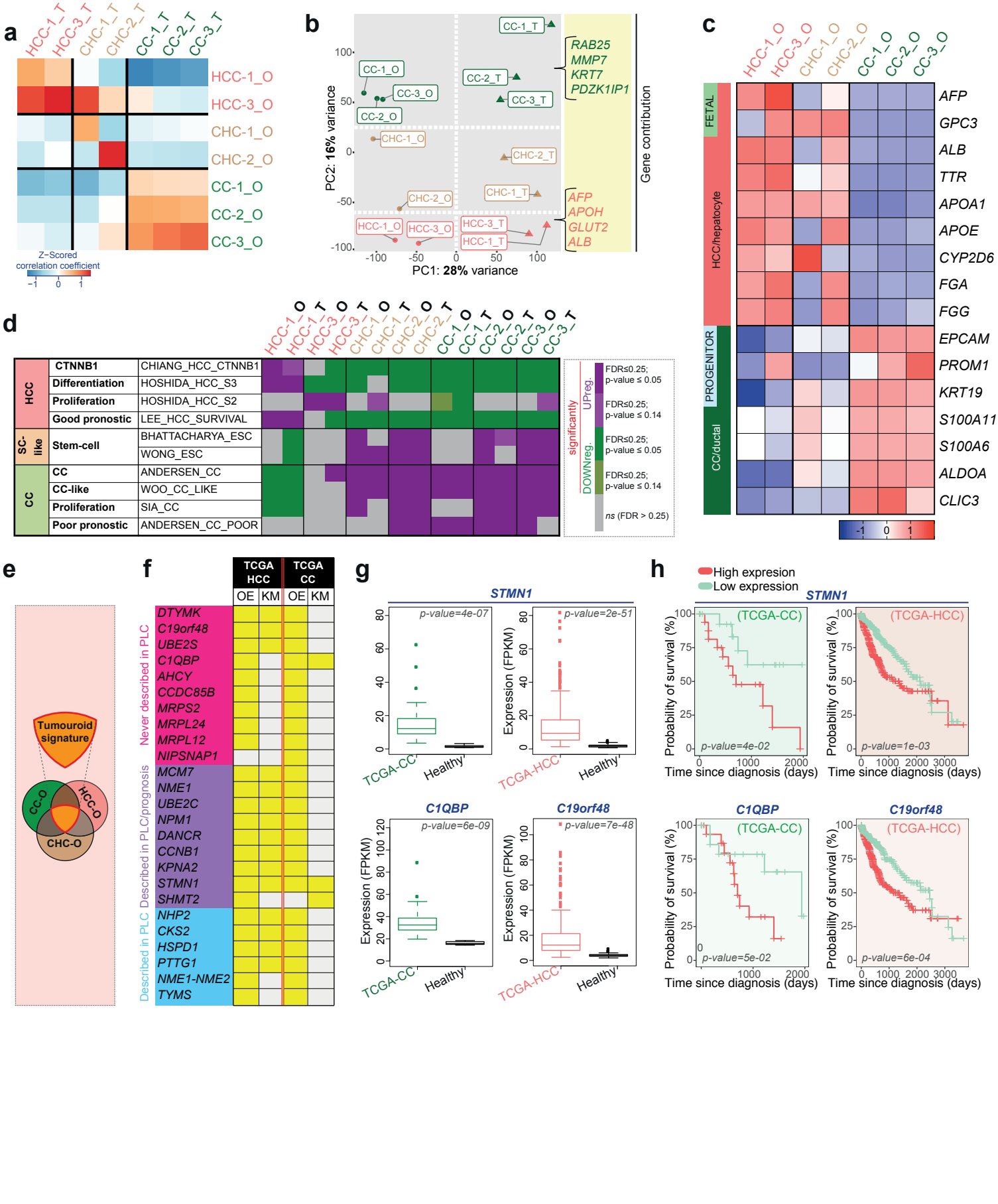
a
HCC-1_T
HCC-3_T
CHC-1_T
CHC-2_T
CC-1_T
CC-2_T
CC-3_T
HCC-1_O
HCC-3_O
CHC-1_O
CHC-2_O
CC-1_O
CC-2_O
CC-3_O
Z−Scored correlation coefficient
−1 0 1
b
PC2: 16% variance
PC1: 28% variance
Gene contribution
RAB25
MMP7
KRT7
PDZK1IP1
AFP
APOH
GLUT2
ALB
c
FETAL
HCC/hepatocyte
PROGENITOR
CC/ductal
AFP
GPC3
ALB
TTR
APOA1
APOE
CYP2D6
FGA
FGG
EPCAM
PROM1
KRT19
S100A11
S100A6
ALDOA
CLIC3
d
CTNNB1
CHIANG_HCC_CTNNB1
Differentiation
HOSHIDA_HCC_S3
Proliferation
HOSHIDA_HCC_S2
Good pronostic
LEE_HCC_SURVIVAL
Stem-cell
BHATTACHARYA_ESC
WONG_ESC
CC
ANDERSEN_CC
CC-like
WOO_CC_LIKE
Proliferation
SIA_CC
Poor pronostic
ANDERSEN_CC_POOR
significantly
UPreg:
DOWNreg:
FDR≤0.25; p-value ≤ 0.05
FDR≤0.25; p-value ≤ 0.14
FDR≤0.25; p-value ≤ 0.05
FDR≤0.25; p-value ≤ 0.14
ns (FDR > 0.25)
e
Tumouroid signature
CC-O
HCC-O
CHC-O
f
TCGA HCC
TCGA CC
OE
KM
Never described in PLC
Described in PLC/prognosis
Described in PLC
DTYMK
C19orf48
UBE2S
C1QBP
AHCY
CCDC85B
MRPS2
MRPL24
MRPL12
NIPSNAP1
MCM7
NME1
UBE2C
NPM1
DANCR
CCNB1
KPNA2
STMN1
SHMT2
NHP2
CKS2
HSPD1
PTTG1
NME1-NME2
TYMS
g
STMN1
p-value=4e-07
p-value=2e-51
Expression (FPKM)
TCGA-CC
TCGA-HCC
Healthy
C1QBP
C19orf48
p-value=6e-09
p-value=7e-48
h
High expresion
Low expression
STMN1
(TCGA-CC)
(TCGA-HCC)
p-value=4e-02
p-value=1e-03
Probability of survival (%)
Time since diagnosis (days)
C1QBP
C19orf48
p-value=5e-02
p-value=6e-04

Figure 4

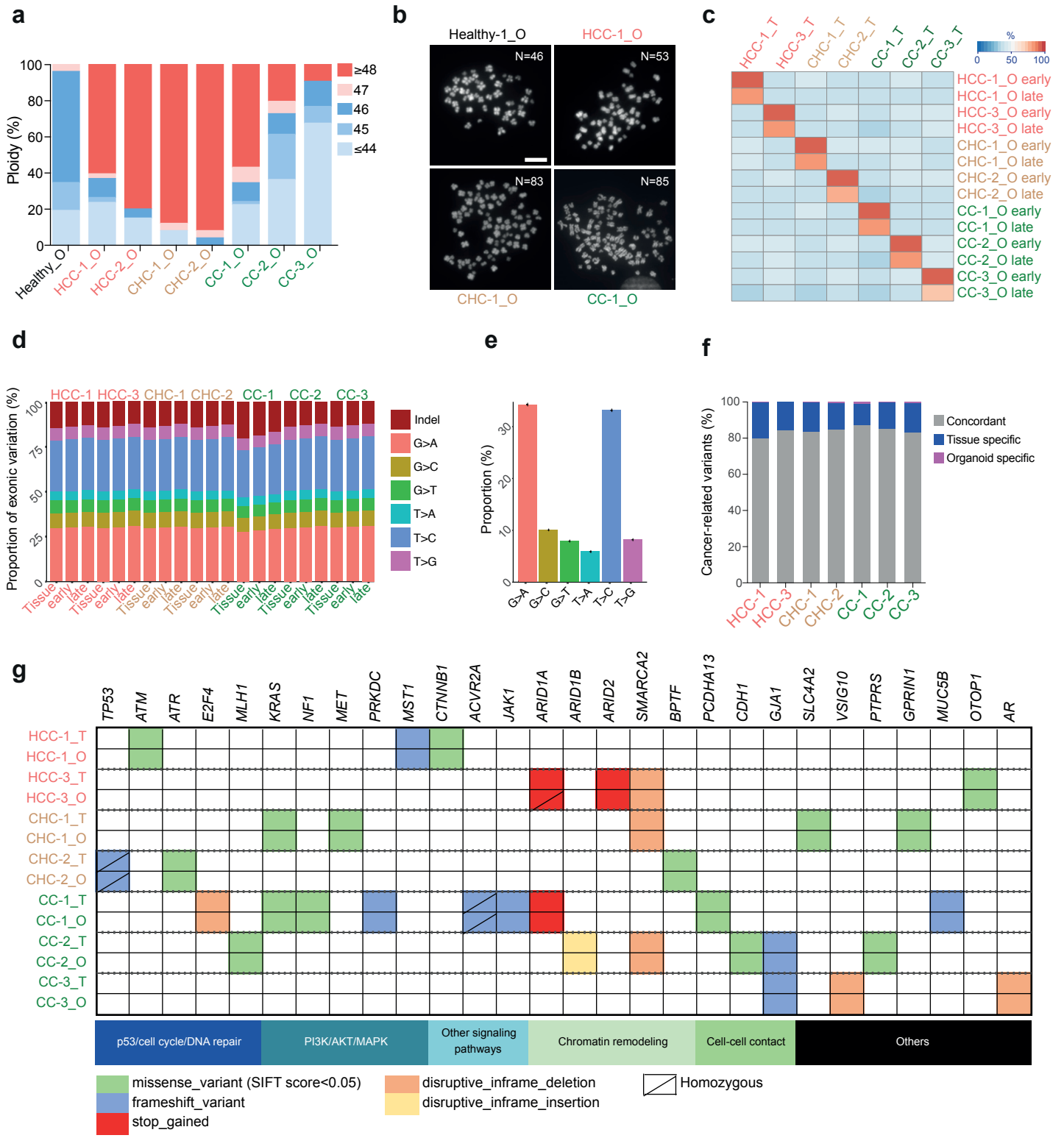
a
Ploidy (%)
≥48
47
46
45
≤44
Healthy_O
HCC-1_O
HCC-2_O
CHC-1_O
CHC-2_O
CC-1_O
CC-2_O
CC-3_O
b
Healthy-1_O
HCC-1_O
N=46
N=53
N=83
N=85
CHC-1_O
CC-1_O
c
HCC-1_T
HCC-3_T
CHC-1_T
CHC-2_T
CC-1_T
CC-2_T
CC-3_T
%
HCC-1_O early
HCC-1_O late
HCC-3_O early
HCC-3_O late
CHC-1_O early
CHC-1_O late
CHC-2_O early
CHC-2_O late
CC-1_O early
CC-1_O late
CC-2_O early
CC-2_O late
CC-3_O early
CC-3_O late
d
Proportion of exonic variation (%)
HCC-1 HCC-3 CHC-1 CHC-2 CC-1 CC-2 CC-3
Indel
G>A
G>C
G>T
T>A
T>C
T>G
e
Proportion (%)
G>A
G>C
G>T
T>A
T>C
T>G
f
Cancer-related variants (%)
Concordant
Tissue specific
Organoid specific
HCC-1
HCC-3
CHC-1
CHC-2
CC-1
CC-2
CC-3
g
TP53
ATM
ATR
E2F4
MLH1
KRAS
NF1
MET
PRKDC
MST1
CTNNB1
ACVR2A
JAK1
ARID1A
ARID1B
ARID2
SMARCA2
BPTF
PCDHA13
CDH1
GJA1
SLC4A2
VSIG10
PTPRS
GPRIN1
MUC5B
OTOP1
AR
p53/cell cycle/DNA repair
PI3K/AKT/MAPK
Other signaling pathways
Chromatin remodeling
Cell-cell contact
Others
missense_variant (SIFT score<0.05)
frameshift_variant
stop_gained
disruptive_inframe_deletion
disruptive_inframe_insertion
Homozygous

Figure 5

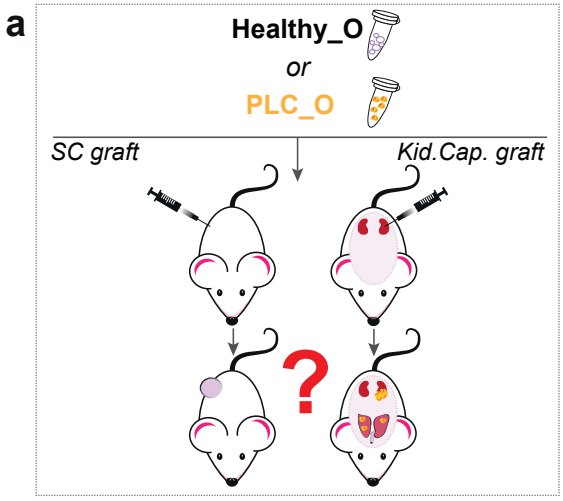

b

	Cells injected	Engraftment	Tumor	Efficiency
CC-1_O	1 000 000	SC	29/29	100%
HCC-1_O	1 000 000	SC	24/34	>70%
Healthy-1_O	1 000 000	SC	0/18	0%

	Cells injected	Engraftment	Tumor	Lung metastasis
CC-1_O	100 000	Kidney capsule	9/9	7/9
Healthy-1_O	100 000	Kidney capsule	0/6	0/6

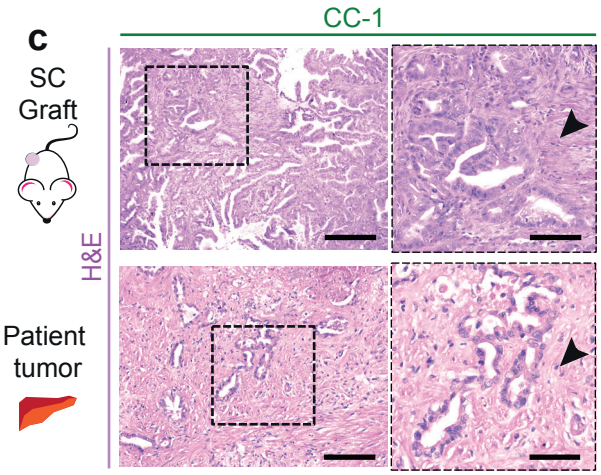

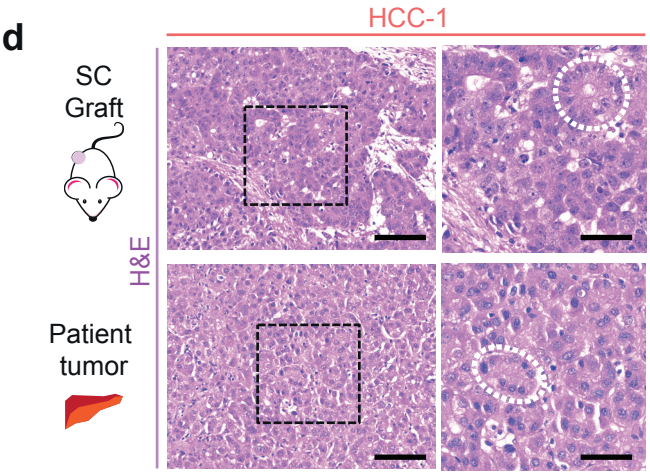

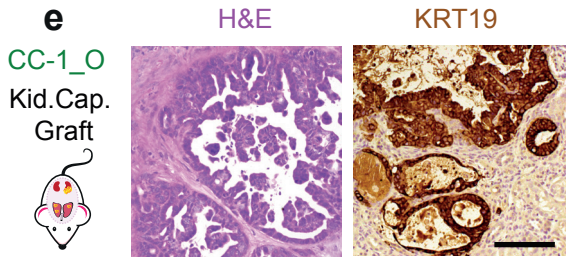

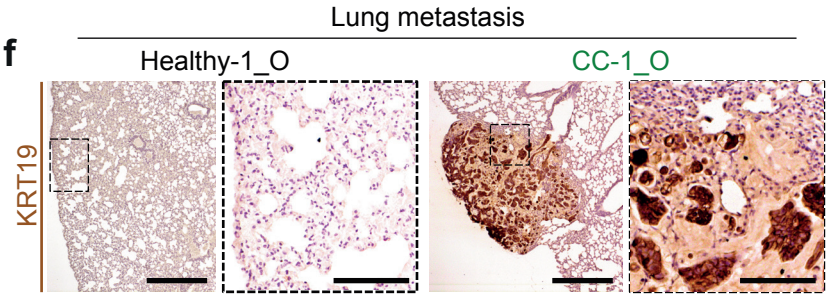

Figure 6

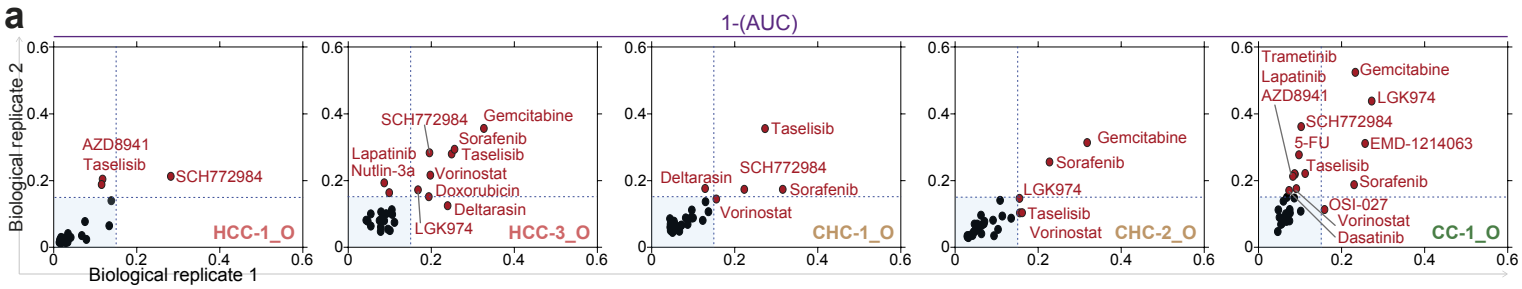

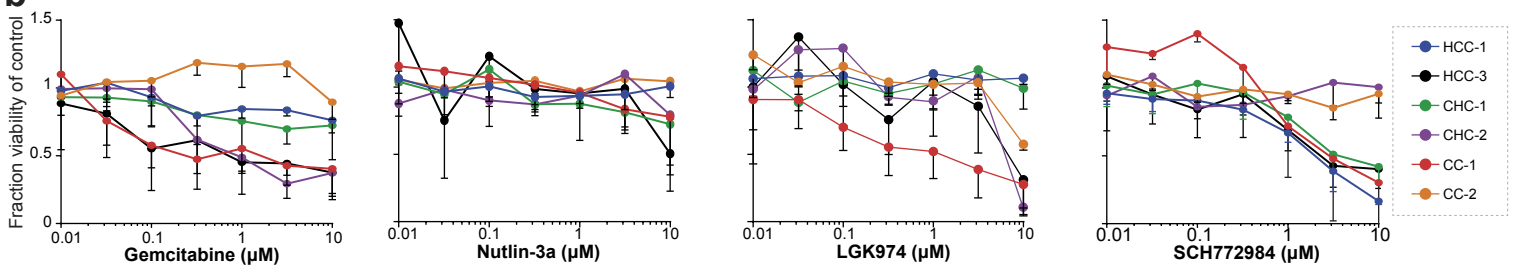

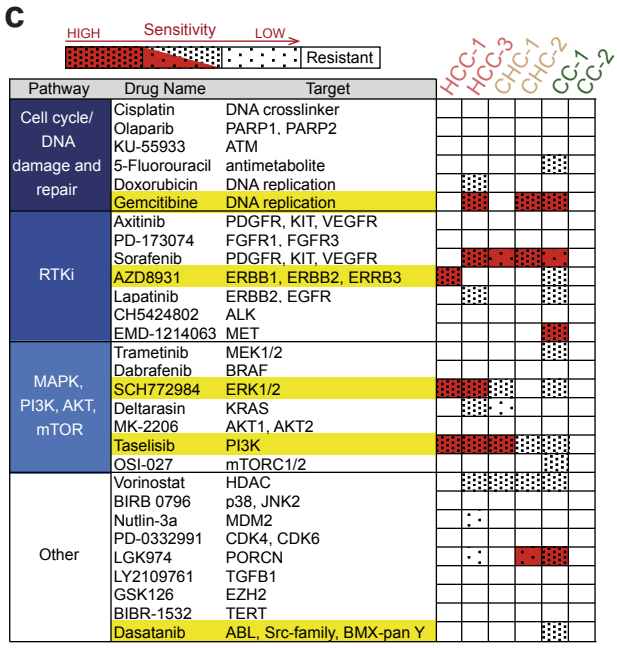

Pathway	Drug Name	Target
Cell cycle/ DNA damage and repair	Cisplatin	DNA crosslinker
	Olaparib	PARP1, PARP2
	KU-55933	ATM
	5-Fluorouracil	antimetabolite
	Doxorubicin	DNA replication
	Gemcitibine	DNA replication
RTKi	Axitinib	PDGFR, KIT, VEGFR
	PD-173074	FGFR1, FGFR3
	Sorafenib	PDGFR, KIT, VEGFR
	AZD8931	ERBB1, ERBB2, ERRB3
	Lapatinib	ERBB2, EGFR
	CH5424802	ALK
	EMD-1214063	MET
MAPK, PI3K, AKT, mTOR	Trametinib	MEK1/2
	Dabrafenib	BRAF
	SCH772984	ERK1/2
	Deltarasin	KRAS
	MK-2206	AKT1, AKT2
	Taselisib	PI3K
	OSI-027	mTORC1/2
Other	Vorinostat	HDAC
	BIRB 0796	p38, JNK2
	Nutlin-3a	MDM2
	PD-0332991	CDK4, CDK6
	LGK974	PORCN
	LY2109761	TGFB1
	GSK126	EZH2
	BIBR-1532	TERT
	Dasatanib	ABL, Src-family, BMX-pan Y

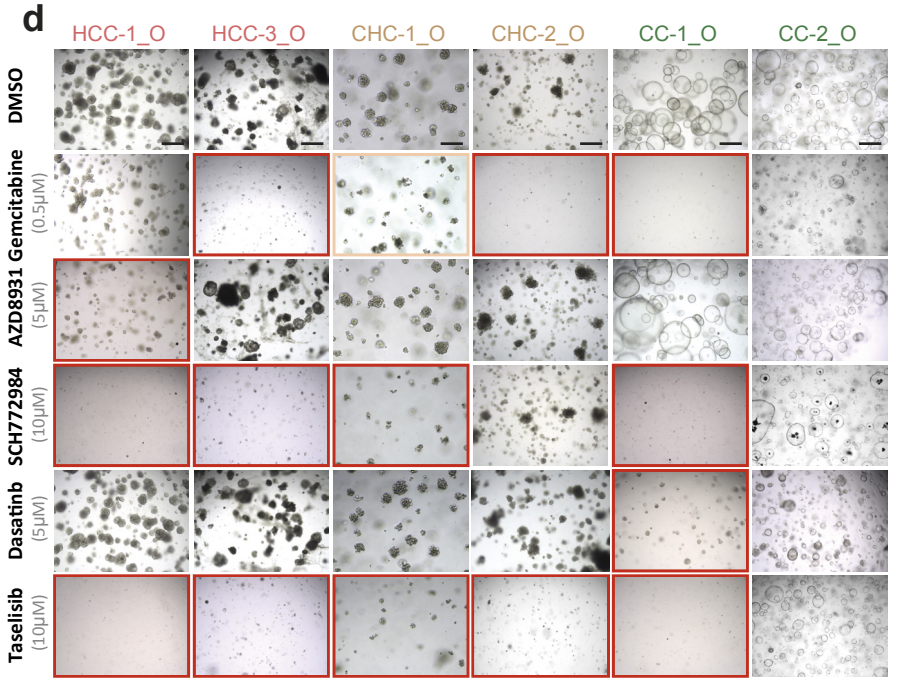

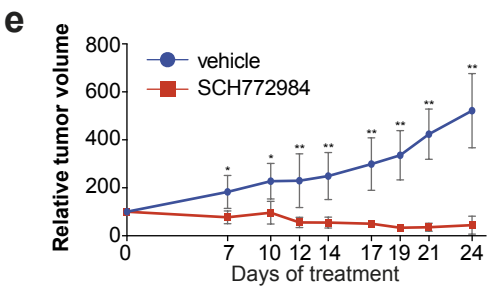

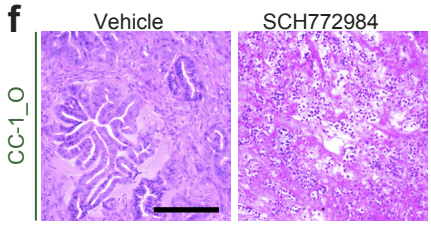

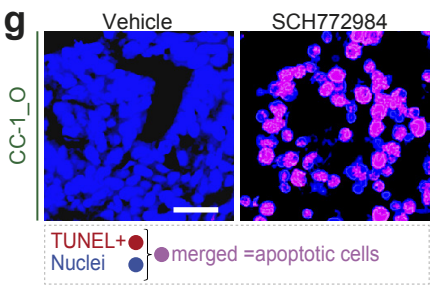

Supplementary Figure 1

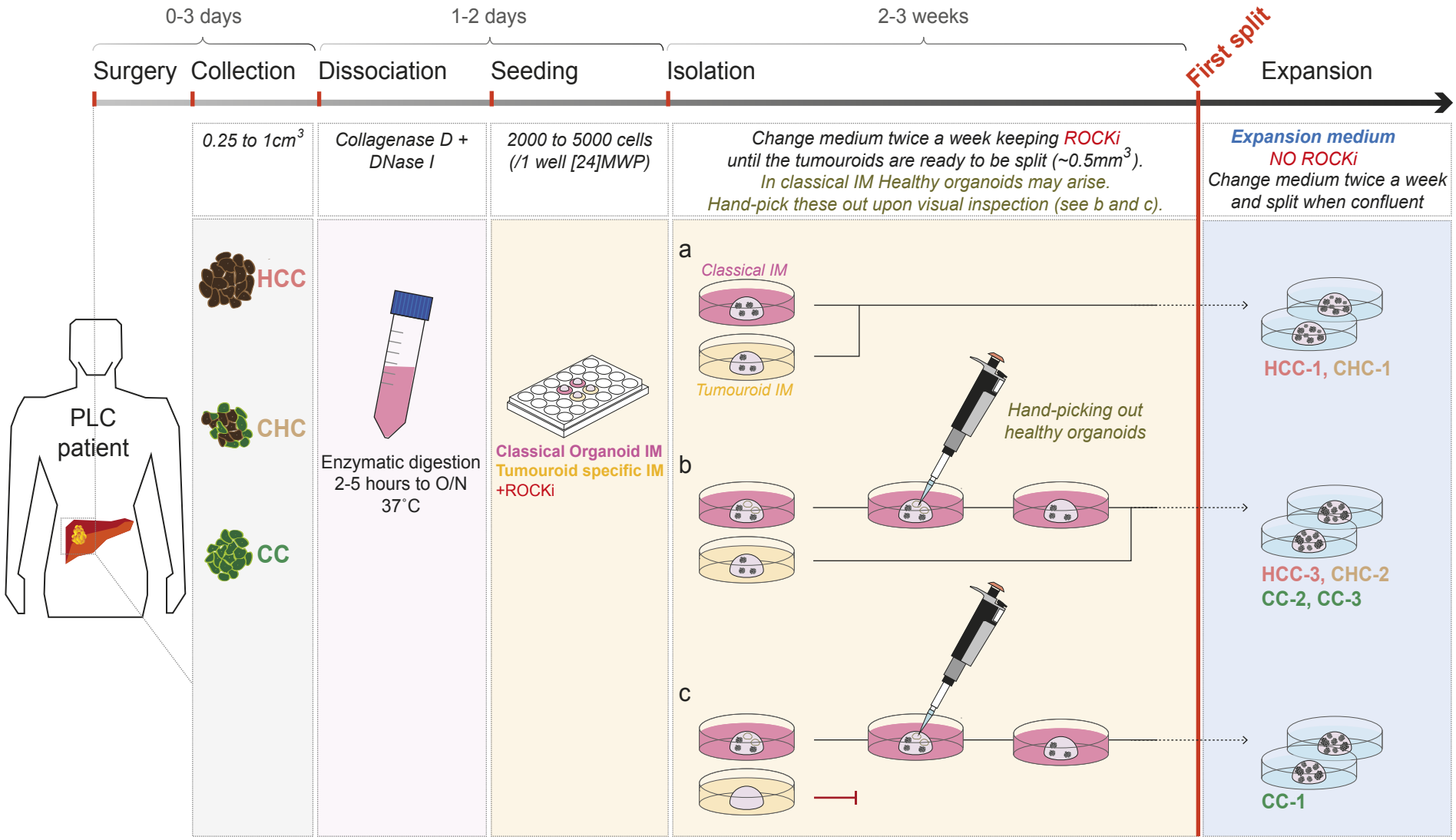

Supplementary Figure 2

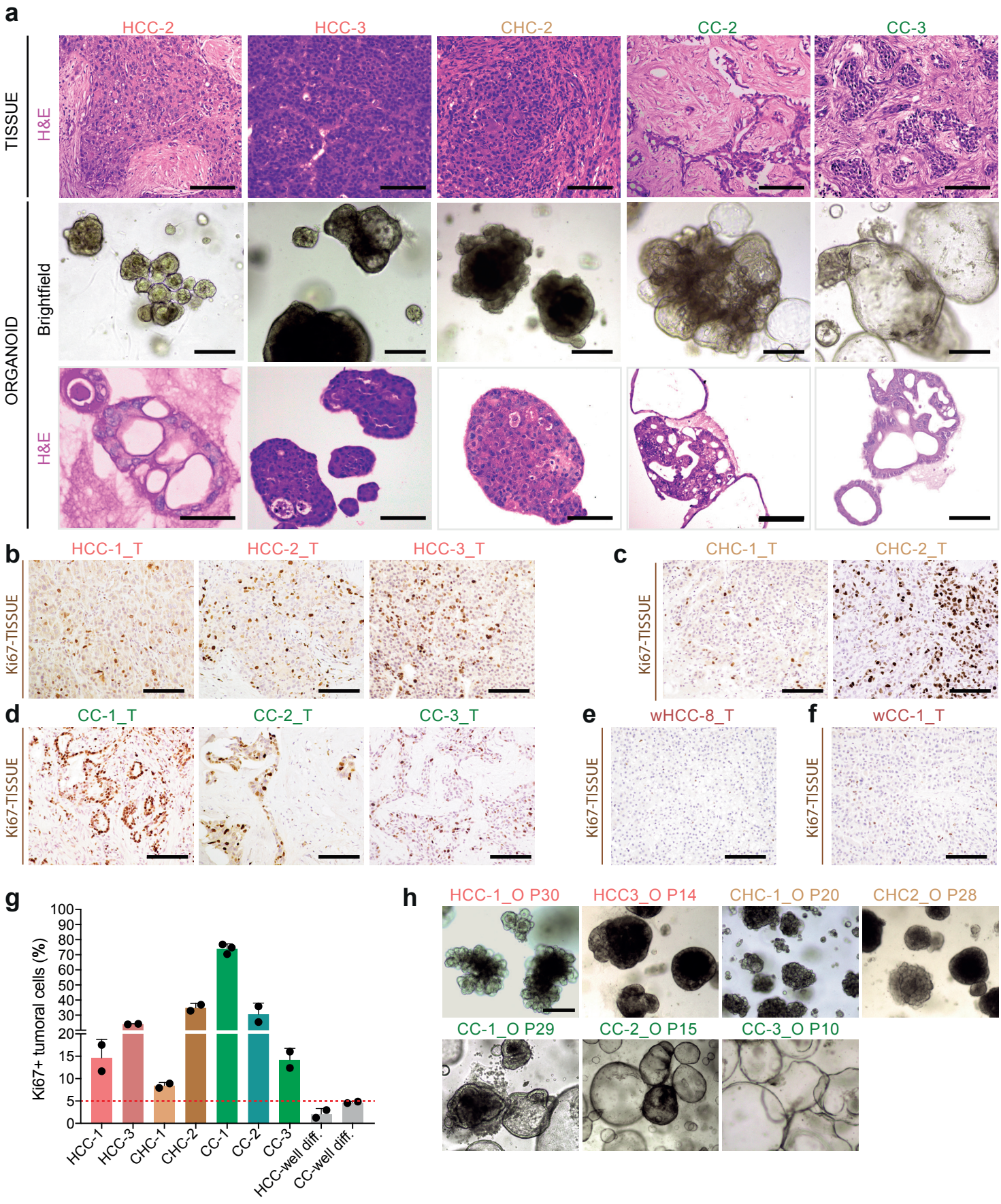

Supplementary Figure 3

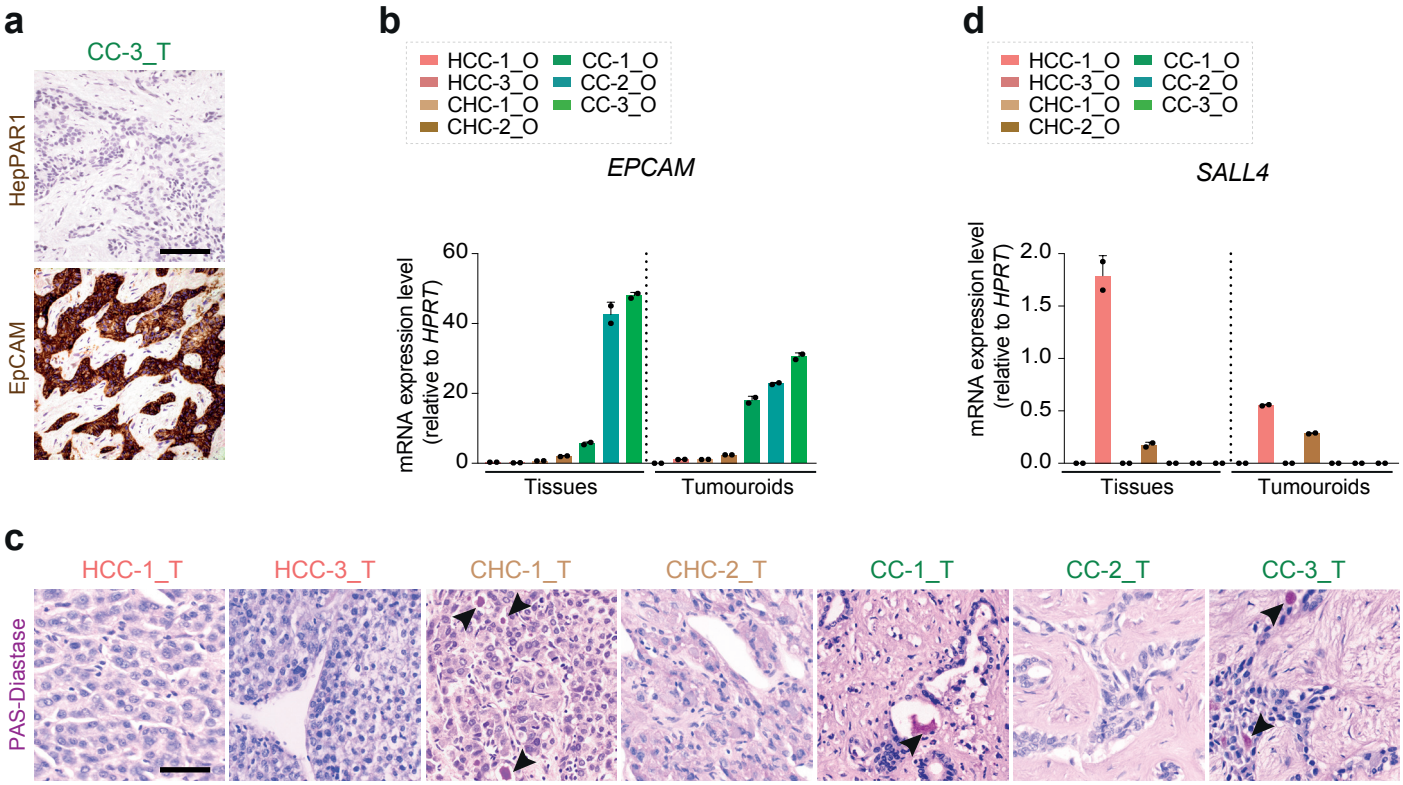

Supplementary Figure 4

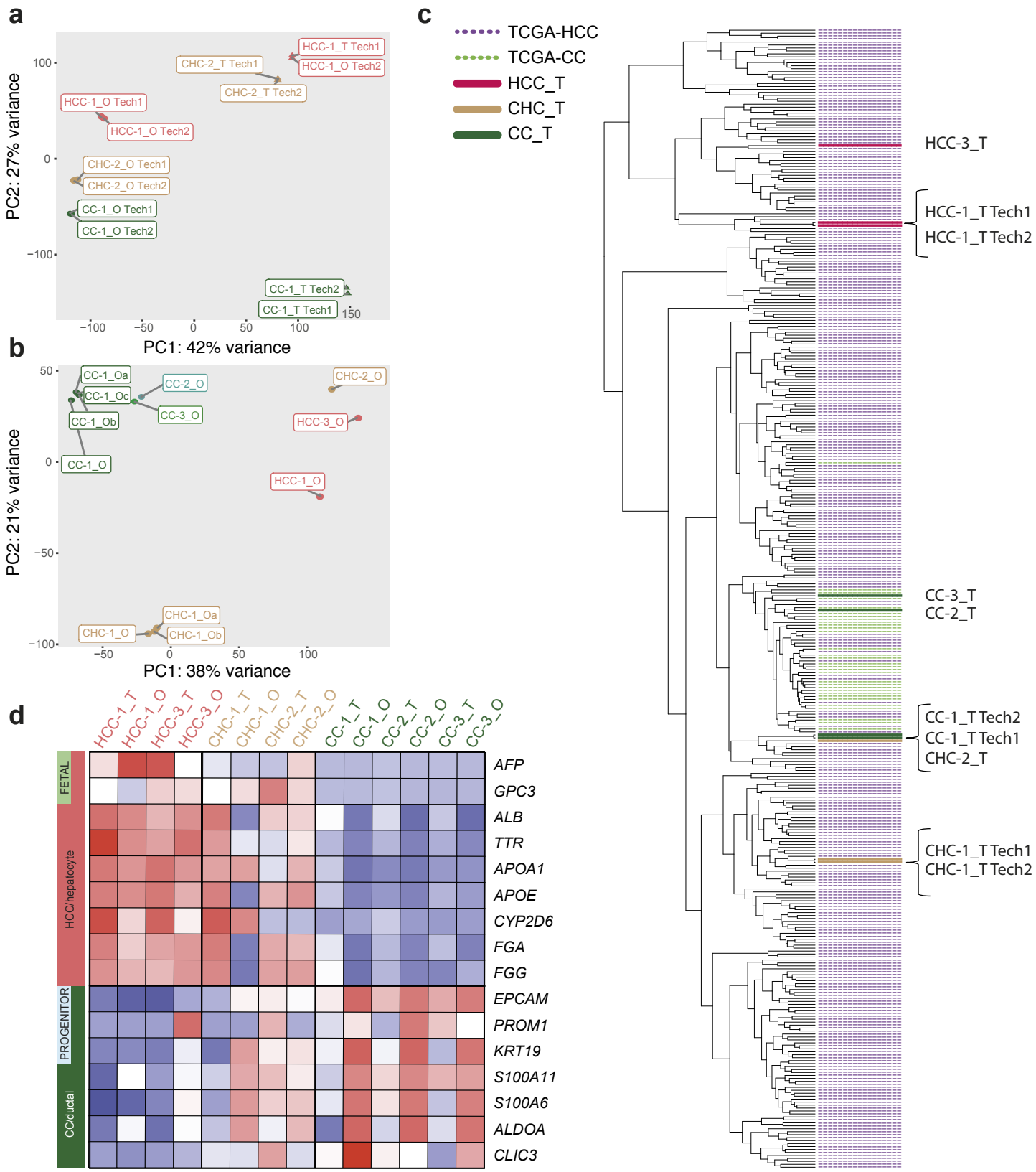

Supplementary Figure 5

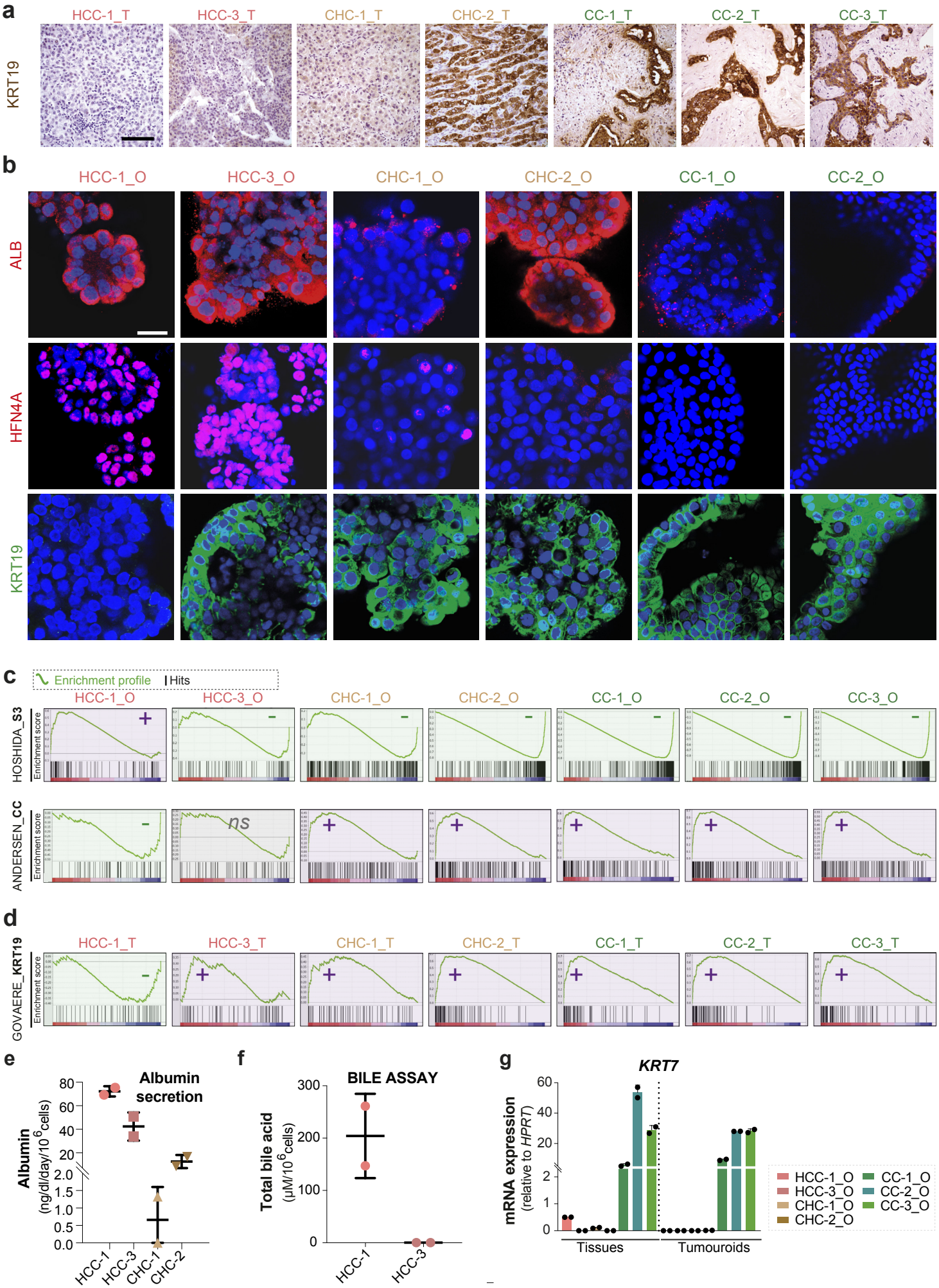

Supplementary Figure 6

a

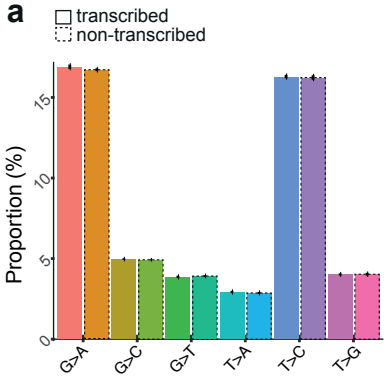

b

		HCC-1	HCC-3	CHC-1	CHC-2	CC-1	CC-2	CC-3
Type of change								
Substitutions								
Coding	Nonsense	2	4	2	1	8	3	6
	Missense	165 (64)	154 (58)	148 (56)	211 (70)	246 (101)	181 (68)	140 (45)
	Structural interaction variant	1 (1)	0	4 (1)	1 (0)	2 (2)	4 (0)	4 (3)
	TOTAL deleterious	***67***	***62***	***59***	***71***	***111***	***71***	***54***
Small insertions and deletions								
Coding		***20***	***17***	***19***	***27***	***183***	***16***	***16***
TOTAL		**87**	**79**	**78**	**98**	**294**	**87**	**70**

SIFT score<0.05 or N/A

c

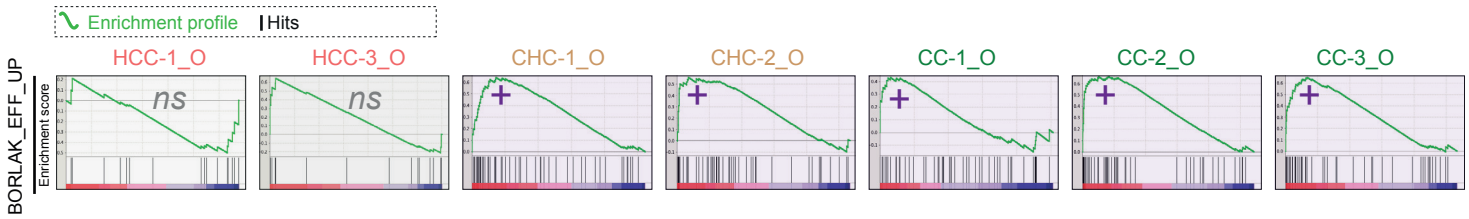

*

a

	Cells injected	Site	Tumor	Efficiency
CC-2_O	1 000 000	SC	8/8	100%
CC-3_O	1 000 000	SC	0/3	0%

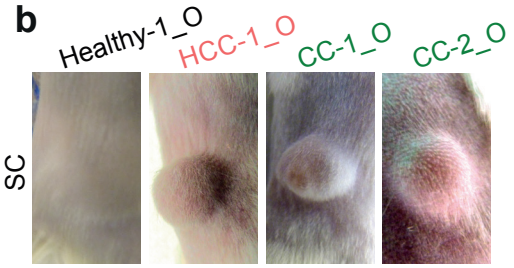

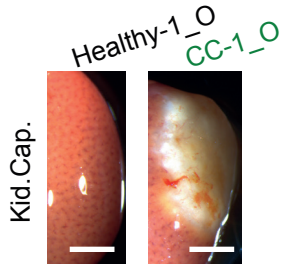

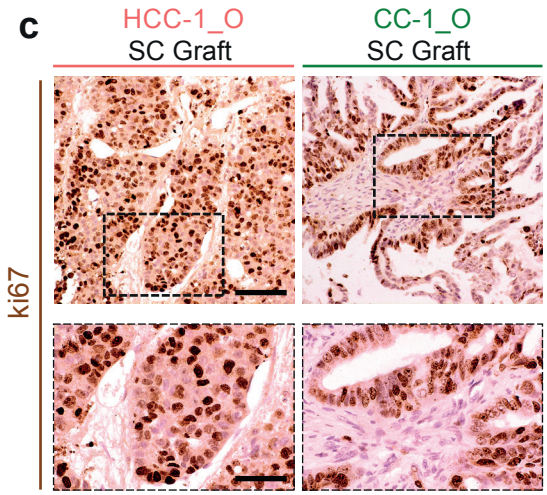

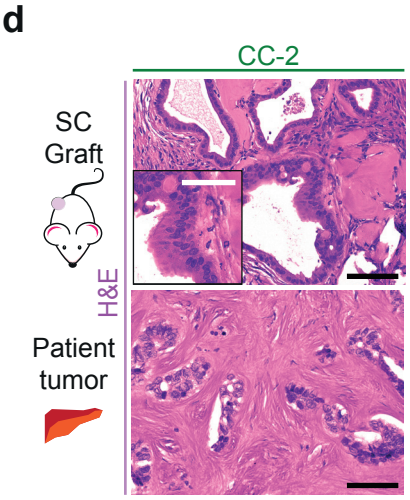

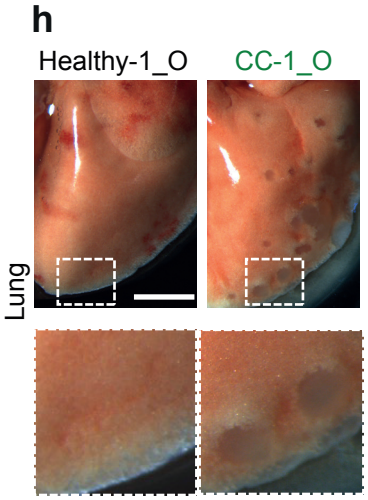

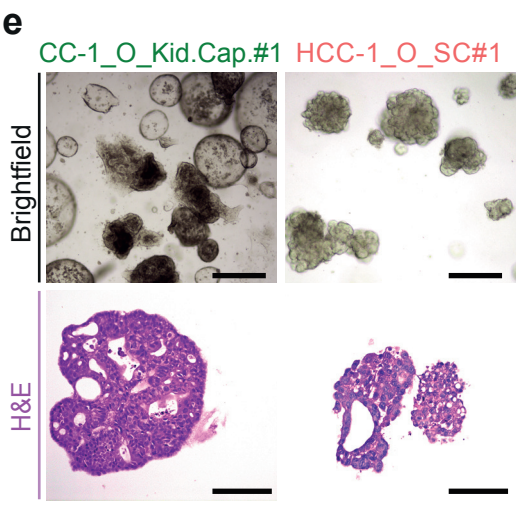

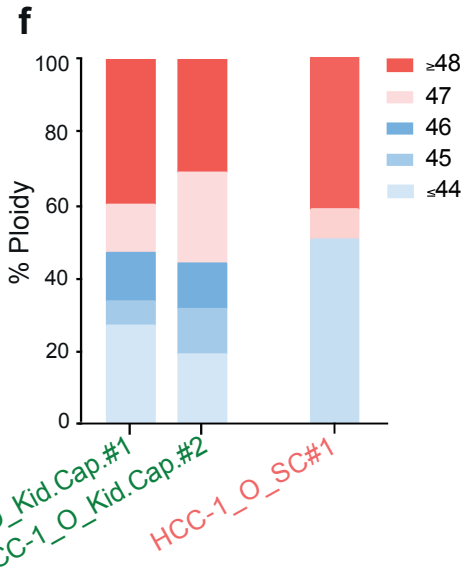

Supplementary Figure 8

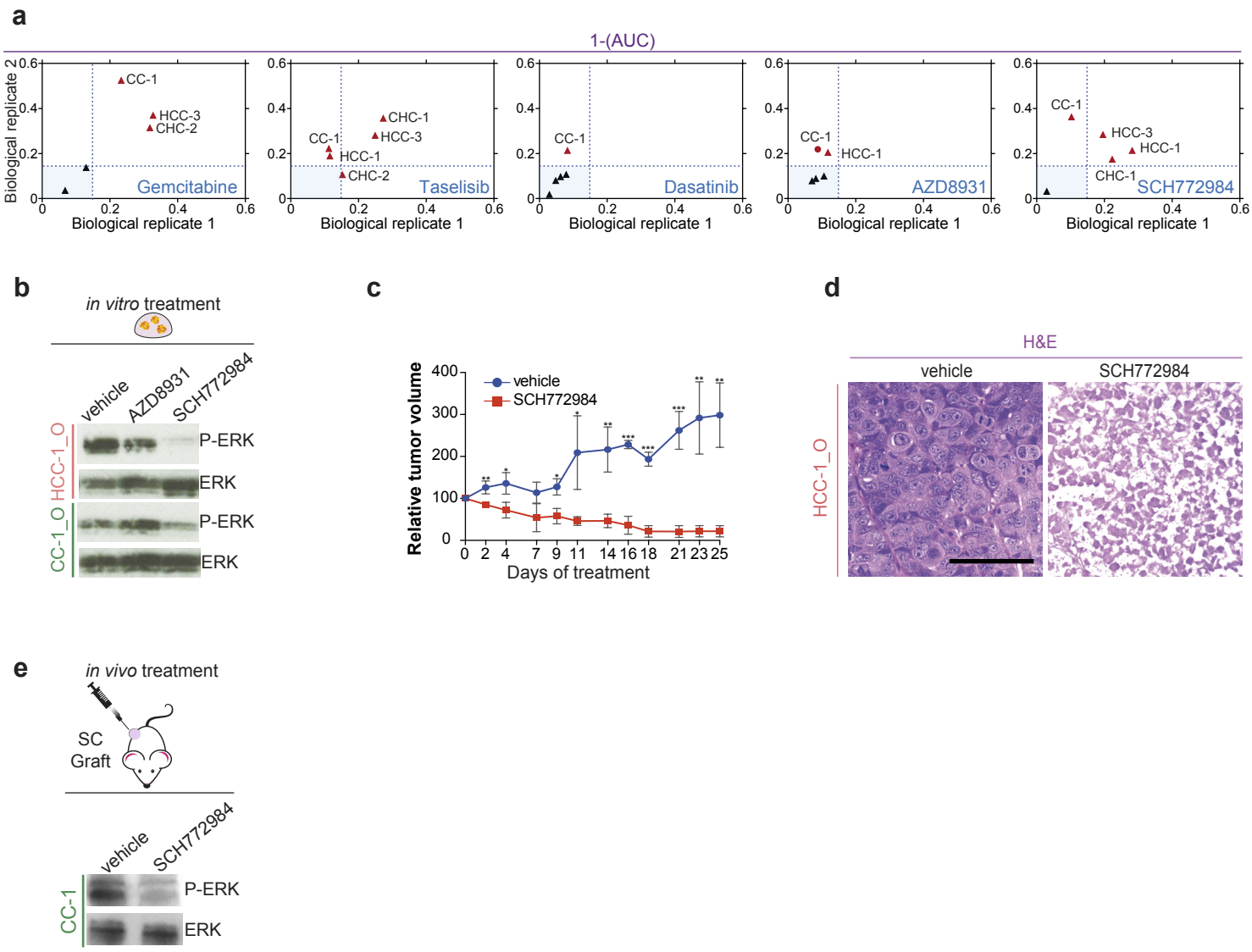

Supplementary Table 1

Sample	Gender	Age	Localisation	Nodal Metastasis	Histological grade	Ki67 index	AFP (µg/L)	Differentiation status	Organoid growth	Organoid expansion	Derivation rate (%)	Expansion rate (%)
CC-1	F	34	Perihilar	Yes	CC mod/well diff.	>5%	2	poorly to moderate/well differentiated	✔	✔	100%	88%
CC-2	M	68	Intrahepatic (segment 5-6)	No	CC mod/well diff.		3		✔	✔		
CC-3	M	64	Intrahepatic (segment 4-5-8)	No	CC poorly diff.		N/T		✔	✔		
CHC-1	F	56	Segment 5	No	CHC - Classical		512		✔	✔		
CHC-2	F	61	Segment 5-6	Yes	CHC - SC		1718		✔	✔		
HCC-1	M	69	Segment 8	No	HCC mod/well diff.		53		✔	✔		
HCC-2	M	52	Segment (2-4), and caudate lobe	No	HCC mod/well diff.		469		✔	x		
HCC-3	F	71	Segment 7	N/A	HCC mod diff.		1700		✔	✔		
HCC-NL1*	F	37	Segment 6	No	HCC mod diff.	N/T	19742	N/A	N/A	N/A	N/A	N/A
wCC-1	F	54	Intrahepatic (4-5)	No	CC well diff.	<5%	N/T	well differentiated	x	x	0%	0%
wHCC-1	M	78	Segment 6	No	HCC well diff.		<2		x	x		
wHCC-2	M	57	Segment 2-3	No	HCC well diff.		6		x	x		
wHCC-3	M	77	Segment 2-3	No	HCC well diff.		2		x	x		
wHCC-4	F	70	Segment 2-3	No	HCC well diff.		2		x	x		
wHCC-5	M	76	Segment 6-7	No	HCC well diff.		N/T		x	x		
wHCC-6	M	75	Segment 2-3-4	No	HCC well diff.		8		x	x		
wHCC-7	M	72	Segment 3	No	HCC well diff.		N/T		x	x		
wHCC-8	M	66	Segement 4B	No	HCC well diff.		7		x	x		
Healthy-1	M	23	Healthy liver; biopsy obtained from donor tissue used for transplantation						✔	✔	100%	100%
Healthy-2	F	44							✔	✔		
Healthy-3	M	50							✔	✔		